Routes to chaos in the periodically driven Lorenz-84 system

Rutger W. Kock

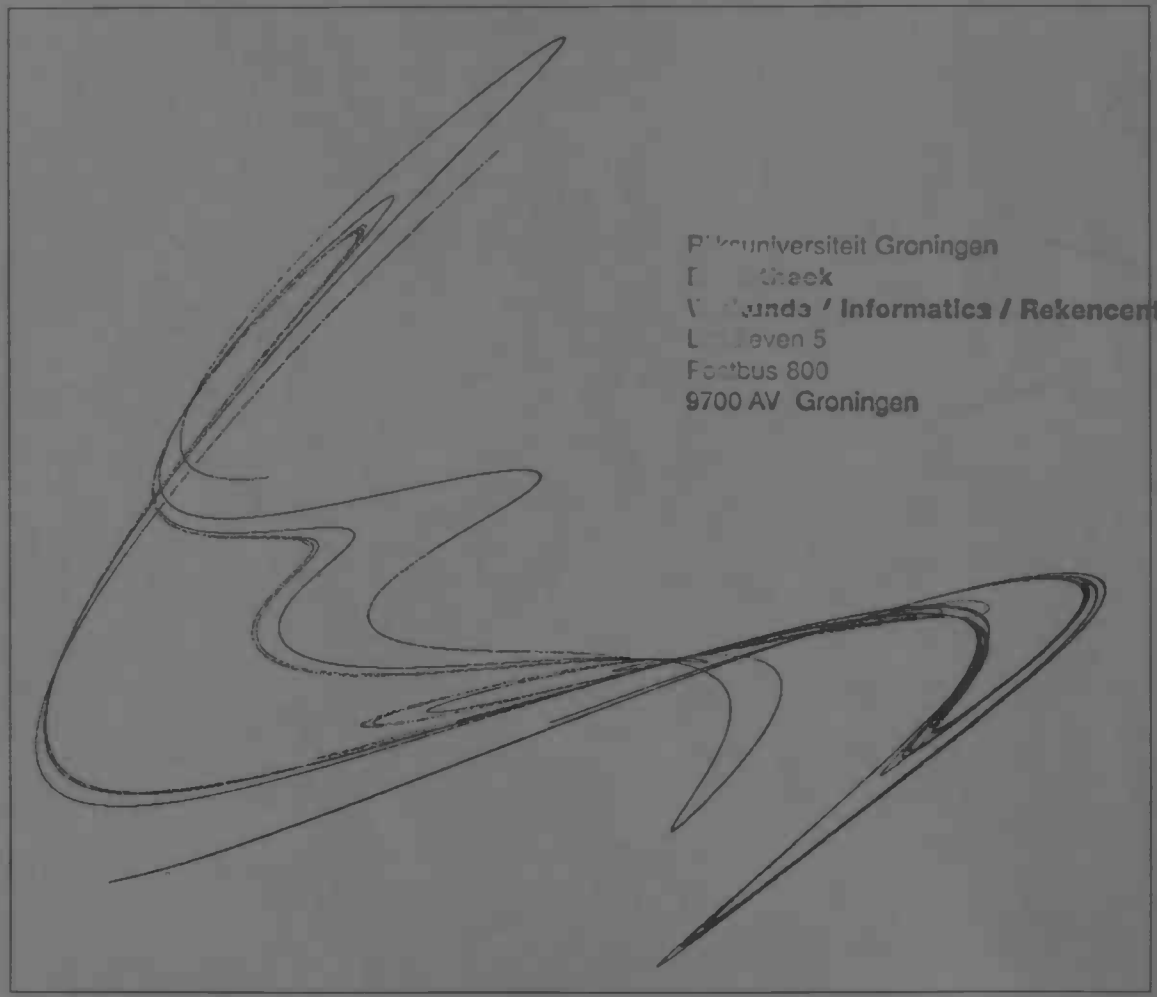

Department of
Mathematics

RuG

Master's thesis

Routes to chaos in the periodically driven Lorenz-84 system

Rutger W. Kock

Advisors:
Prof.dr. H.W. Broer and Dr. I. Hoveijn
Rijksuniversiteit Groningen
Department of Mathematics
Postbus 800
9700 AV Groningen

August 1998

Preface

This paper has been written as a master thesis under the supervision of prof.dr. H. W. Broer and dr. I. Hoveijn at the University of Groningen.
It is the result of a joint project of the Dynamical Systems group at the University of Groningen, the Predictability group of the KNMI at De Bilt and the Dynamical Systems group at the University of Utrecht. The research has been done partly at the University of Groningen and partly at the Predictability group at the KNMI.
I wish to thank Henk Broer and Igor Hoveijn for their enthousiastic supervision. I learned a lot from them.
Furthermore I wish to thank dr. J.D. Opsteegh and the KNMI for their hospitality and prof. dr. F. Verhulst of the University of Utrecht for his interest.
Further I wish to thank prof. Simó in Barcelona for his suggestions and giving me some of his numerical results concerning the driven Lorenz-84 system. Krista Homan for our valuable cooperation and Florian Wagener, Bernd Krauskopf and the Dynamical Systems group in Groningen for their interest.
Finally I wish to thank my parents, my brothers, my grandma and my friends for always keeping faith in me.

Contents

1 Introduction

1.1 The model: the driven Lorenz-84 system

The long-term behaviour of the weather is unpredictable. To get a better understanding it is important to know which scenarios cause the unpredictability. Modern computer models, which for example *KNMI* uses for the daily weather prediction, are so complicated (high dimension, many parameters) that it is impossible to find the cause of unpredictability. That is why it is suggested to deduce a simplified model with qualitatively similar properties. Then geometric methods from the theory of dynamical systems can be used to investigate the appearing routes to chaos, chaos being the qualitative equivalent of the above unpredictability. In 1984 Lorenz [21] introduced an autonomous low-order model of the large scale atmospheric circulation in the Northern Hemisphere, obtained by a suitable truncation of the infinite dimensional Navier-Stokes equations, the so called geostrophic equations. It is a climate system with mainly large-scale effects both in space and in time. This 3-dimensional system of nonlinear ordinary differential equations is given by

$$\begin{aligned} \dot{X} &= -Y^2 - Z^2 - aX + aF \\ \dot{Y} &= XY - bXZ - Y + G \\ \dot{Z} &= bXY + XZ - Z \end{aligned}$$

where the independent variable t represents time. The variable X represents the strength of a large-scale westerly-wind current zonal flow. This strength is proportional to the meridional temperature gradient. The variables Y and Z represent respectively the amplitudes of the cosine and sine phases of the first order mode in a Fourier-expansion of large scale superposed waves. The parameter F represents a forcing of the westerly current due to the north-south temperature gradient, while G represents a forcing by the continent-ocean temperature contrast. The dynamics of this system is thoroughly investigated by Anastassiades [1], Broer, Homan, Hoveijn and Krauskopf [4], Homan [16] and Shil'nikov et al. [32] with F and G as control parameters. However, the north-south temperature gradient, F, is smaller in summer than in winter and also the continent-ocean temperature contrast, G, varies. To study these seasonal effects we replace F and G by periodic parameters

$$F = F_0(1 + \varepsilon \cos \omega t) \quad \text{and} \quad G = G_0(1 + \varepsilon \cos \omega t)$$

so turning Lorenz-84 into a parametrically forced system referred to as *the driven Lorenz-84 system*.

$$\begin{aligned} \dot{X} &= -Y^2 - Z^2 - aX + aF_0(1 + \varepsilon \cos \omega t) \\ \dot{Y} &= XY - bXZ - Y + G_0(1 + \varepsilon \cos \omega t) \\ \dot{Z} &= bXY + XZ - Z \\ \dot{t} &= 1 \end{aligned}$$

$a = \frac{1}{4}$ and $b = 4$ are set as constants, see Lorenz [21]. By putting $T = \frac{2\pi}{\omega}$ this 4-dimensional system is T-periodic in t where the time unit is estimated to be five days. This system is

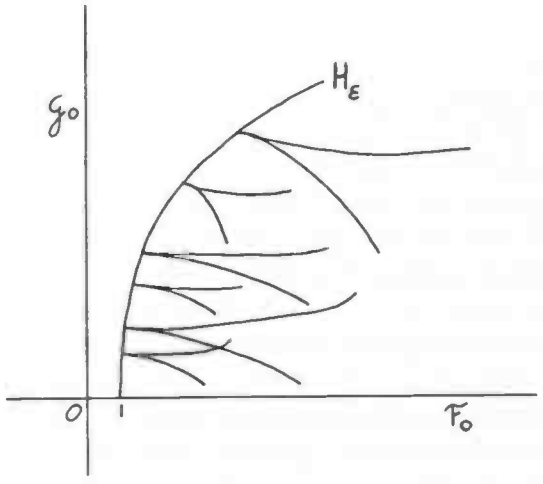

Figure 1: Driven Lorenz-84 system: Sketch of the Hopf curve H_ε with emerging Arnol'd resonance tongues of the 3D-Poincaré map $f_{T,\varepsilon,\alpha}$ for $\varepsilon \neq 0$ in the (F_0, G_0)-plane.

mainly investigated with control parameters $\alpha := (F_0, G_0)$ for various fixed values of T and ε. But sometimes also ε is varied. This driven system can be seen as a simplification of a coupled atmospheric-oceanic model as was investigated by Zondervan [33] and will be investigated in current and future research of the *KNMI* in cooperation with the *RUU*.

1.2 Setting of the problem

The main interest is how complicated, chaotic phenomena in the dynamics of driven Lorenz-84 are generated out of simple phenomena. Therefore bifurcations of the limit sets are considered, upon variation of the parameters $\alpha = (F_0, G_0)$. Especially the influence of forcing on the generation of chaotic phenomena is investigated. The system with $\varepsilon = 0$, the Lorenz-84 system, is the starting-point for the investigations of the driven system ($\varepsilon \neq 0$). These systems are compared with each other in a numerical perturbation analysis.
From a meteorological point of view, the periods $T = 73$ and $T = 0.2$ are most relevant. Since the time unit is estimated to be five days, these periods correspond respectively to one year and one day.
In our method of study we consider a 3-dimensional Poincaré map $f_{T,\varepsilon,\alpha}$ of the 4-dimensional system. The definition of this Poincaré map is given in section 2.1. Our investigations are guided by results of Lorenz-84 which are presented in section 3. Theoretical expectations for the dynamics of the driven Lorenz-84 system are made on the basis of these results, see section 4. Of main interest are bifurcations or cascades of bifurcations, especially those leading to chaotic behaviour. There are several of such routes to chaos. For example accumulation of tongue boundaries or other mechanisms which destroy an invariant circle. The latter are found inside Arnol'd tongues. Thus we concentrate on their boundaries and special points thereof. Examples are cusps and dovetail bifurcations, see Broer, Simó and Tatjer [7]. Arnol'd resonance tongues emerge from a curve of Hopf bifurcations of fixed points of $f_{T,\varepsilon,\alpha}$, see figure 1 for a sketch. For ε small this curve is expected to be near a corresponding Hopf curve of equilibria of Lorenz-84.

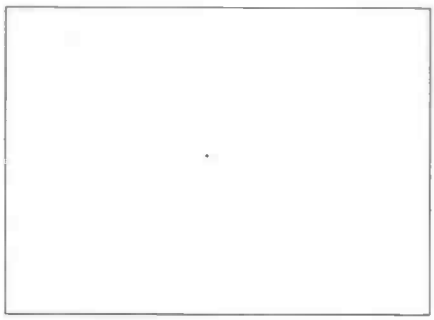

(a) $(F_0, G_0) = (6, 7.9)$
Fixed point repellor

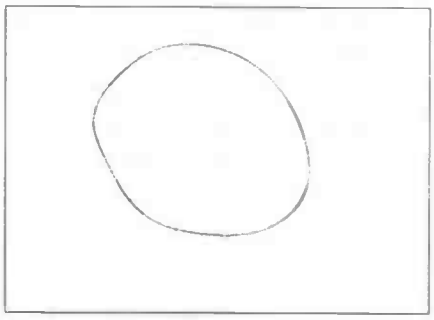

(b) $(F_0, G_0) = (13.3, 7.9)$
Quasi-periodic behaviour on circle repellor

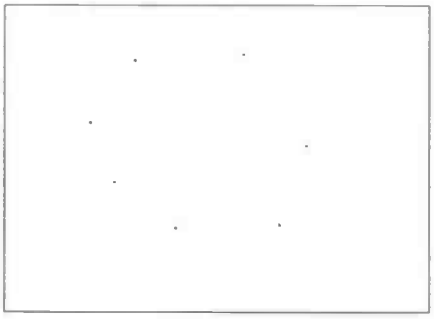

(c) $(F_0, G_0) = (13.5, 7.9)$
Period 7 orbit on circle repellor

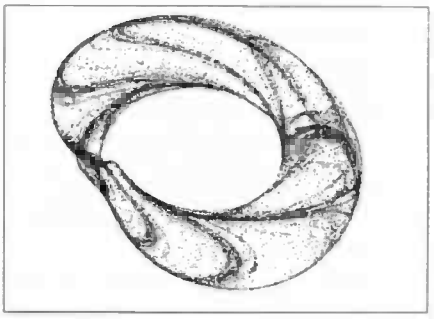

(d) $(F_0, G_0) = (14.5, 7.3)$
Chaotic repellor

Figure 2: Driven Lorenz-84 system with $T = 0.5$ and $\varepsilon = 0.1$: Projection of repellors of 3-dimensional Poincaré map $f_{\varepsilon,\alpha}$ with different values of $\alpha = (F_0, G_0)$ onto (Y, Z)-plane of seize $(-2.5, 2.5) \times (-1, 3)$.

These theoretical expectations determine the direction of our numerical explorations. Attractors and repellors of the Poincaré map $f_{T,\varepsilon,\alpha}$ are found by numerical investigation using the software package `DsTool` [14]. A numerical bifurcation analysis of the 4-dimensional vector field is done with `AUTO` [11]. However the detected bifurcations are presented as bifurcations of the 3-dimensional map $f_{T,\varepsilon,\alpha}$. The results of these explorations are compared with the theoretical expectations. Finally conclusions and new expectations are given.

1.3 Summary of the results

The driven Lorenz-84 system is numerically investigated for the periods $T = 73$ (year rhythm), $T = 0.2$ (day rhythm) and $T = 0.5$. For F_0 and G_0 small the dynamics is simple and the only limit sets of the Poincaré map $f_{T,\varepsilon,\alpha}$ are fixed points. If $G_0 = 0$ a simple analytic solution exists on the F_0-axis: $(X(t), Y(t), Z(t)) = (F_0(1 + \varepsilon \cos \omega t), 0, 0)$ corresponding to the fixed point $(X, Y, Z) = (F_0(1 + \varepsilon), 0, 0)$ of the Poincaré map $f_{T,\varepsilon,(F_0,0)}$. The influence of forcing varies for different periods. Figure 2 illustrates of the appearance of all sorts of dynamics

in the driven Lorenz-84 system. Arnol'd resonance tongues are found in the (F_0, G_0)-plane at the right hand side of the Hopf curve, H_ε. Their boundaries are continued with help of AUTO [11] in the (F_0, G_0)-plane for fixed values of ε and in the (G_0, ε)-plane for fixed values of F_0. These tongues agree with the theoretical expectations in the neighbourhood of H_ε as ε is small. Also codimension 2 and 3 bifurcations, for example cusps and dovetail bifurcations are found on the tongue boundaries. Furthermore a route to chaos by overlapping of Arnol'd resonance tongues is found. Chaotic repellors appear around a broken-up circle repellor. The results of the numerical investigation of the driven system with $T = 0.5$ are presented in section 7.

The driven Lorenz-84 system with year rhythm $T = 73$ appears hard to investigate with AUTO [11] and DsTool [14]. This is due to numerical problems as the integration time to get the next iterate of the Poincaré map is quite large. However we will present some results C. Simó obtained by using an in this case more accurate integration routine. These results indicate the existence of very narrow Arnol'd resonance tongues emerging at the right hand side of the Hopf curve H_ε. These tongues structure a large area of the parameter plane, as G_0 is relative small compared to F_0. If we increase the value of G_0 chaotic behaviour is seen. However at a certain value of G_0 (depending on F_0) the dynamics becomes simpler again. First the circle attractor reappears and for G_0 larger there is a fixed point attractor, which persists for G_0 even larger. These results are discussed in section 5.

In a numerical investigation with AUTO [11] and DsTool [14] of the driven Lorenz-84 system with day rhythm, $T = 0.2$, no qualitative differences are detected with Lorenz-84. for example Arnol'd resonance tongues appear to be so narrow that numerically no frequency locking is found, see section 6.

The first exploration of the driven Lorenz-84 system shows that the system has rich and complicated dynamics. The results suggest further studies in different areas, most fruitful will be a mixture of theoretical and numerical studies, see Broer, Simo and Tatjer [7]. The suggestions are listed below.

1. Unfolding of the codimension 2 and 3 bifurcations on the Arnol'd tongue boundaries, see for example the results obtained for the fattened Arnol'd family by Broer, Simó and Tatjer [7].

2. Unfolding of the codimension 3 cusp saddle-node bifurcation, as detected at the boundaries of the Arnol'd tongue with $\rho = \frac{3}{5}$ in the driven Lorenz-84 system with $T = 0.5$, see figure 30.

3. Unfolding of the codimension 2 period-doubling saddle-node bifurcation, as detected at on the boundaries of the Arnol'd tongue with $\rho = \frac{3}{5}$ in the driven Lorenz-84 system with $T = 0.5$, see figure 36.

4. Looking for 3D chaotic attractors, their theory is in progress by Tatjer.

Finally it is needed to get a derivation of the Lorenz-84 model from the Navier-Stokes equations for a better meteorological interpretation of the results. Saltzman did some work on this subject, see [31].

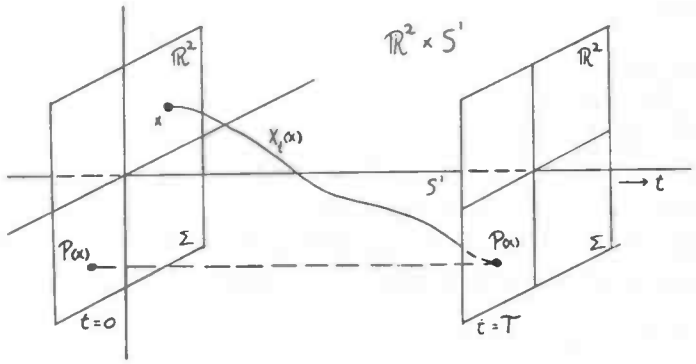

Figure 3: Poincaré or stroboscopic map P in the case of a 3D T-periodic vector field X in 3D.

2 Theory

In this section some theory of dynamical systems is reviewed as far as it is used to investigate the driven Lorenz-84 system. First, the Poincaré map is explained and defined for the driven Lorenz-84 system. Second the relation between this map and the original system is given. Third a brief overview is presented of bifurcations of maps. The rotation number ρ of an invariant circle is defined and the phenomenon Arnol'd tongue is introduced. Finally some routes to chaos are discussed.

2.1 The Poincaré map

The driven Lorenz-84 system is a 4 dimensional vector field, X, which is T-periodic in time. To analyze the system we want to decrease the dimension of the system but not lose information. Therefore we make use of the time-periodicity of X and define the following cross section of dimension 3

$$\Sigma = \{(x,t) \in \mathbb{R}^3 \times \mathbb{R}/T\mathbb{Z} \mid t = 0 \bmod(\mathrm{T}\mathbb{Z})\} \simeq \mathbb{R}^3.$$

The flow $X_t(x)$ of X is everywhere transverse to Σ, because $\dot{t} = 1 > 0$, $\forall t$. So we define the following (global) *Poincaré (return) map* on Σ by

$$f_{T,\varepsilon,\alpha} : \Sigma \to \Sigma \quad , \quad f_{T,\varepsilon,\alpha}(x) = X_T(x),$$

with $X_T(x)$ the "T-flow" of the vector field starting at the point $x \in \Sigma$.
This Poincaré (return) map is also called a *stroboscopic map*. See figure 3 for a 2 dimensional Poincaré map in the case of a 3 dimensional vector field that is a T-periodic function of t.
Every attractor, respectively repellor of the driven Lorenz-84 system has a corresponding attractor, repellor of $f_{T,\varepsilon,\alpha}$ in Σ. Fixed points of $f_{T,\varepsilon,\alpha}$ correspond to T-periodic solutions of the system, while period k-points define sub harmonics of period kT. Invariant circles of $f_{T,\varepsilon,\alpha}$ correspond to invariant 2-tori (possibly carrying quasi-periodic solutions), while irregular invariant sets correspond to chaotic oscillations.

2.2 Bifurcations

In this subsection we give a brief overview of some bifurcations of a fixed point x_α of the map $f_\alpha : \mathbb{R}^n \to \mathbb{R}^n$. As parameters are varied changes may occur in the qualitative structure of the limit sets of the map f_α. These changes are called *bifurcations*. The *codimension* is the number of parameters necessary to encounter (and describe) such a bifurcation in a family of maps. Bifurcations that can be detected by looking at any small neighbourhood of a fixed point are called *local* bifurcations , the others are called *global*.
The stable and unstable invariant manifolds of the fixed point x_α are defined as

$$W^s(x_\alpha) = \{x \in \mathbb{R}^n : f_\alpha^k(x) \to x_\alpha, k \to \infty\},$$

respectively

$$W^u(x_\alpha) = \{x \in \mathbb{R}^n : f_\alpha^k(x) \to x_\alpha, k \to -\infty\}.$$

These manifolds play an important role in global bifurcations.

2.2.1 Local bifurcations

We define

$$B_\alpha := D_{x_\alpha} f_\alpha(x_\alpha)$$

as the linearisation of f_α around a fixed point x_α. A local bifurcation of x_α occurs if one or more eigenvalues of B_α cross the unit circle. A bifurcation is called *super-critical* if the fixed point x_α is weakly stable. A bifurcation is called *sub-critical* if the fixed point x_α is weakly unstable.
We only describe the super-critical bifurcations. For the (corresponding) sub critical cases we refer to Guckenheimer and Holmes [13] and Kuznetsov [19].
The eigenvectors corresponding to the eigenvalues that cross the unit circle span the center manifold $W^c(x_\alpha)$. The bifurcations are discussed in this center manifold.
For definitions of technical terms (weakly stable, hyperbolicity, center manifold), see Guckenheimer and Holmes [13] and Kuznetsov [19].

1. **Codimension 1 bifurcations for maps**

   (a) **Saddle-node bifurcation**
   A saddle-node bifurcation, SN, occurs if B_α has a simple real eigenvalue $\mu_1 = 1$. A fixed point of saddle-type and a stable fixed point collide and disappear. The center manifold has dimension 1. See figure 4 for this bifurcation.

   (b) **Period-doubling bifurcation**
   A period-doubling bifurcation, PD, occurs if B_α has a simple real eigenvalue $\mu_1 = -1$. A stable period p orbit becomes unstable and a stable period $2p$ orbit appears. The center manifold has dimension 1. See figure 5 for this bifurcation.

   (c) **Hopf bifurcation for maps**
   A Hopf bifurcation, H, occurs if B_α has a simple pair of complex conjugate eigenvalues on the unit circle, $\mu_{1,2} = e^{\pm 2\pi i\psi}$, $0 < \psi < \frac{1}{2}$, with $\mu_{1,2}^k \neq 1$, for $k \in \{1,2,3,4\}$. A stable fixed point becomes unstable and an attracting invariant circle appears. The center manifold has dimension 2. See figure 6 for this bifurcation. For $k \in \{1,2,3,4\}$ codimension 2 bifurcations occur, see below.

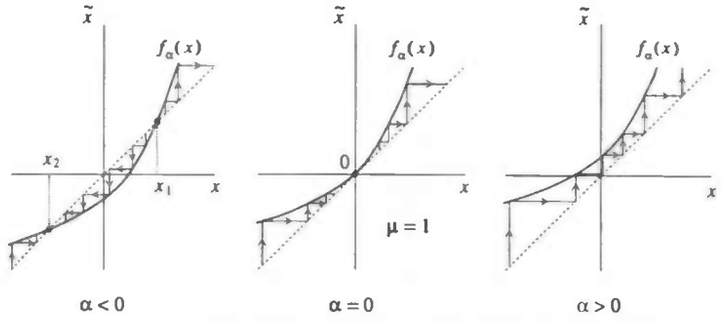

Figure 4: Saddle-node bifurcation at $\alpha = 0$, the variable x parameterizes the 1D center manifold, Kuznetsov [19].

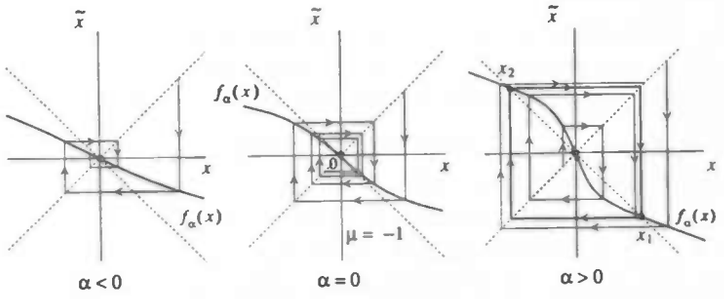

Figure 5: Period doubling bifurcation at $\alpha = 0$, the variable x parameterizes the 1D center manifold, Kuznetsov [19].

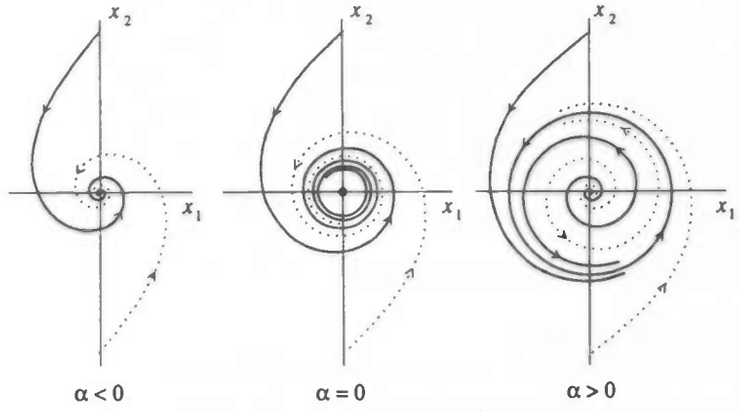

Figure 6: Hopf bifurcation for maps at $\alpha = 0$, the variables x_1 and x_2 parameterize the 2D center manifold, Kuznetsov [19].

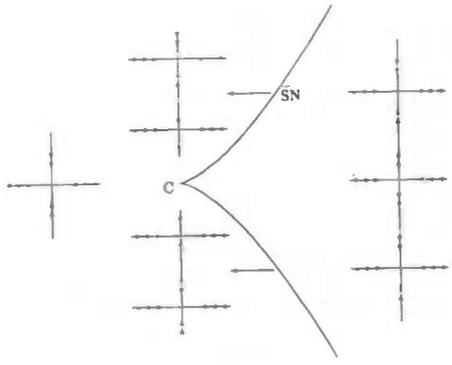

Figure 7: Cusp bifurcation, Broer, Simó and Tatjer [7].

2. **Codimension 2 bifurcations for maps**

   (a) **Cusp bifurcation**
   A cusp bifurcation, C, is a degenerate saddle-node bifurcation. In the parameter plane the cusp generically is a point where two saddle-node curves meet tangentially, see figure 7. The center manifold has dimension 1.

   (b) **Hopf-saddle-node bifurcation for maps**
   A Hopf-saddle-node bifurcation, HSN, occurs if B_a has a simple pair of complex conjugate eigenvalues on the unit circle, $\mu_{1,2} = e^{\pm 2\pi i\psi}$, $0 < \psi < \frac{1}{2}$, with $\mu_{1,2}^k \neq 1$, for $k \in \{1,2,3,4\}$ and another eigenvalue $\mu_3 = 1$. In a parameter plane this is a point where a curve of saddle-node bifurcations is tangent to a curve of Hopf bifurcations. For the unfolding of this bifurcation in the case of vector fields see Guckenheimer and Holmes [13] and Kuznetsov [19]. The center manifold has dimension 3.

   (c) **Strong resonances**
   An $1 : k$ strong resonance, with $k \in \{1,2,3,4\}$, occurs if B_a has a simple pair of complex conjugate eigenvalues on the unit circle, $\mu_{1,2} = e^{\pm 2\pi i\psi}$, $0 < \psi < \frac{1}{2}$ and $\mu_{1,2}^k = 1$. The Hopf curve is destroyed at these points. The center manifold has dimension 2. The first strong resonance, $k = 1$, is also called a Bogdanov-Takens bifurcation, BT. For more information about these bifurcations in general, see Arnol'd [2], Kuznetsov [19] and Guckenheimer and Holmes [13]. For information about the BT bifurcation in particular, see Broer et al. [6]. For information about 1:4 resonance in particular, see Krauskopf [17].

3. **Codimension 3 bifurcations for maps**

   (a) **Dovetail bifurcation**
   A dovetail bifurcation is a degenerate cusp bifurcation. Such as the cusp bifurcation is a degenerated saddle-node bifurcation. See figure 8 for a dovetail area. See Broer, Simó and Tatjer [7] for more details.

Remark
Not only fixed points can undergo bifurcation, also invariant circles can. For example an

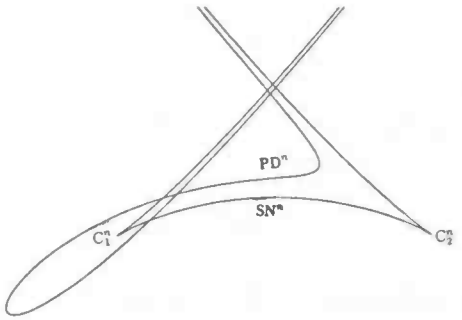

Figure 8: Dovetail area, Broer, Simó and Tatjer [7].

invariant circle S can undergo a period doubling bifurcation thereby creating an invariant circle $2S$ of double length. These (special) bifurcations are called *quasi-periodic bifurcations*, see for more information Broer, Huitema and Sevryuk [5].

2.2.2 Global bifurcations

Let x_0, x_1 and x_2 be a fixed points of saddle-type of the map f_α. The point x is called *homoclinic* to x_0 if

$$f^n(x) \to x_0, \quad t \to \pm\infty.$$

The point x is called *heteroclinic* to x_1 and x_2 if

$$f^n(x) \to x_1, \quad t \to \infty \qquad \text{and} \qquad f^n(x) \to x_2, \quad t \to -\infty.$$

We only discuss homoclinic (tangency) bifurcations. For heteroclinic (tangency) bifurcations we refer to Guckenheimer and Holmes [13] and Kuznetsov [19].

1. **Homoclinic (tangency) bifurcation**
   Let x be a point that is homoclinic to the fixed point x_0 of saddle type. In x the invariant manifolds $W^s(x_0)$ and $W^u(x_0)$ generically intersect transversally. The intersection at x implies an infinite number of intersections of the manifolds at the points $f^{(n)}(x)$, $n \in \mathbb{Z}$, see figure 9 (left) and also figure 14 (right). Such a structure implies the presence of an infinite number of (high) periodic orbits and also chaotic orbits near this homoclinic orbit, see sub-subsection 2.5.2. However at a certain parameter value, say $\alpha = 0$, the invariant manifolds can become tangent and after this no longer intersect. This bifurcation involves an infinite number of SN and PD bifurcations at which the periodic and chaotic orbits will disappear. The homoclinic tangency bifurcation is illustrated in figure 9.

2.3 Rotation number

The rotation number is defined for an orbit of a map f on an invariant circle S. Mostly the rotation number of $f : S \to S$ is defined by

$$\rho = \frac{1}{2\pi} \lim_{k\to\infty} \frac{f^{(k)}(\phi) - \phi}{k},$$

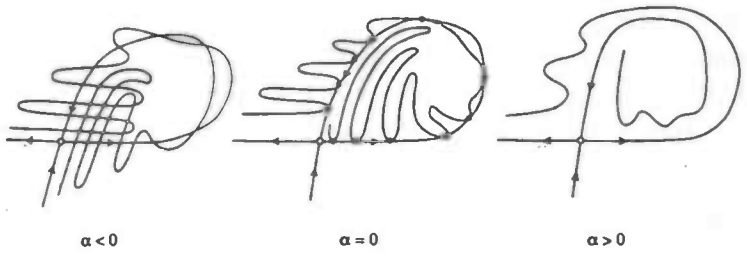

Figure 9: Homoclinic tangency bifurcation at $\alpha = 0$, Kuznetsov [19].

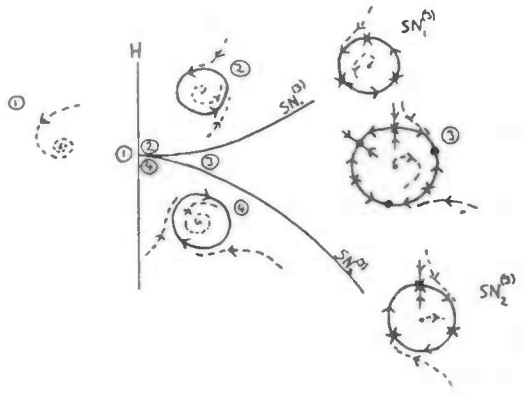

Figure 10: Unfolding around a (p,3) resonance point on the Hopf curve: an Arnol'd tongue.

with $\phi \in S$. The role of the rotation number is clarified by the following lemma:

Lemma 1 *The rotation number of the map $f : S \mapsto S$ is rational, $\rho = \frac{p}{q}$, if and only if f has a (p, q)-periodic orbit.*

Remark
For practical purpose the rotation number of an invariant circle of the map $f_{T,\varepsilon,\alpha}$ is approximated by putting

$$\rho = \frac{T}{P_{(F,G)}}$$

With T the period of the forcing and $P_{(F,G)}$ the period of the limit cycle at the right hand side of the Hopf curve, H, in the (F, G)-plane of the autonomous case, see subsection 3.2. This is in practice a good approximation for $\varepsilon \ll 1$. The Hopf curve in the (F_0, G_0)-plane of the map $f_{T,\varepsilon,\alpha}$, with ε small, is expected to be close to H of the autonomous case. Furthermore, close to the curves in the parameter plane where the autonomous system has period RT we expect points where the map $f_{T,\varepsilon,\alpha}$ has rotation number R.

2.4 Arnol'd tongues

We consider the (Poincaré) map, $f_\alpha : \mathbb{R}^n \to \mathbb{R}^n$ with $\alpha \in \mathbb{R}^2$ and $n \geq 2$. Assume that there is a curve of super-critical [1] Hopf bifurcations in the parameter plane. When crossing such

[1] The sub-critical case is similar, just change attracting by repelling.

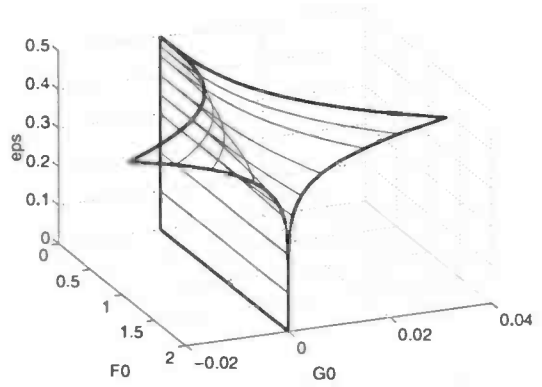

Figure 11: 3 dimensional Arnol'd tongue in the (F_0, G_0, ε)-parameter space.

a curve transversally, an invariant circle will appear. The dynamics on such a circle depends strongly on the place of crossing the Hopf curve.
At points on the Hopf curve where the rotation number $\rho = \frac{p}{q}$ with $p, q \in \mathbb{Z}$ but $q \neq 1, 2, 3, 4$ narrow parameter regions emerge where the dynamics on the attracting invariant circle is periodic, see figure 10 [2]. Such a region is called an *Arnol'd resonance tongue*. For parameter values inside a tongue a period-q attractor and a period-q orbit of saddle-type exist on the circle. These orbits persist under small parameter variations, so the tongue is open. The rotation number is rational and constant inside a tongue. The tongues are bordered by two curves of saddle-node bifurcations, $SN^{(q)}$, where the period-q attractor and the period-q orbit of saddle-type collide and disappear through a saddle-node bifurcation. Outside the tongues the dynamics is quasi-periodic. ρ is irrational and so an orbit fills up the invariant circle densely, e.g. see Devaney [10], §1.3, Theorem 3.13.
The phenomenon of a periodic orbit on an invariant circle is also called *frequency locking*.
In the case of 3 parameters, a 3 dimensional Arnol'd tongue may exist in the parameter space. Intersections between this 3 dimensional tongue and appropriate planes give the "usual" (2 dimensional) Arnol'd tongue. It is expected that in the (F_0, G_0, ε) parameter space of the map $f_{T,\varepsilon,\alpha}$ the width w, of the 3 dimensional Arnol'd tongues with rotation number $\rho = \frac{p}{q}$ at distance d of a relevant Hopf bifurcation plane behaves like

$$w_\varepsilon(d) \simeq d^{\frac{q}{2}} c(\varepsilon)$$

with $0 < \varepsilon \ll 1$ and $c(\varepsilon) = O(\varepsilon^k)$ for all k, i.e. $c(\varepsilon)$ is smaller than any polynomial in ε.

On basis of this estimate a schematic view of a 3 dimensional Arnol'd tongue in parameter space is made, see figure 11. Furthermore the estimate expresses the following:

1. The smaller the denominator of the rotation number the larger the Arnol'd tongue. So numerical investigations will be concentrated first on tongues with $q = 5$.

2. For $\varepsilon < 1$ also the larger tongues remain small in the neighbourhood of the Hopf curve.

[2] Actually $q = 3$ gives a strong resonance but this value is chosen to make figure 10 more clear.

How the width of the Arnol'd tongues depends on the period of forcing T is not known. However when T is about as big as the characteristic periods of the autonomous Lorenz-84 system the most influence of T is expected.

2.5 Routes to chaos

In this section several routes to chaos which may occur in the map $f_\alpha : \mathbb{R}^n \to \mathbb{R}^n$ with $\alpha \in \mathbb{R}^2$ and $n \geq 2$ are briefly discussed. In the first sub-subsection we concentrate on routes to chaos via the destruction of an invariant circle inside Arnol'd tongues. In the following sub-subsection the period doubling route is presented.

2.5.1 Destruction of the invariant circle

For parameter values inside the Arnol'd tongue the invariant circle may lose its smoothness, due to the lack of normal hyperbolicity. An invariant circle is called normal hyperbolic [3] if the attraction of nearby orbits *to* the invariant circle is stronger than the attraction of points *on* the invariant circle.
In general an invariant circle, S, becomes less smooth at further distance of the Hopf curve and finally breaks up. When S is destroyed it can turn into an irregular invariant set near a homoclinic structure formed by the intersection of the stable and unstable manifolds of the periodic orbit of saddle-points on S. The invariant set of this map plays the same role as the closed invariant 'Cantor' set of the Horseshoe map [4]. So in this invariant set are located:

1. A countable infinite number of (high) periodic orbits of saddle type,
2. an uncountable set of bounded non periodic (chaotic) orbits, which lay dense in the invariant set.

This irregular set can be in a small neighbourhood of the saddle point giving occurrence to small Hénon like strange attractors, see Palis and Takens [25]. But it is also possible that the irregular set is draped around the former invariant circle. Then "large" chaotic attractors appear which are also called *Viana attractors*, see Broer, Simó and Tatjer [7] and references therein. The chaotic attractor is the closure of the unstable manifold of a saddle point, just as the Hénon attractor is, see figure 12.
Some ways in which an invariant circle may lose its smoothness are given below.

1. Changing of the stability of a fixed or periodic point on the invariant circle, S.
   (a) The periodic point x_α on S can turn from a *node* into a *focus*. That is two real eigenvalues, $\mu_{1,2}$, become complex conjugate. In this way the circle would only be a continuous curve. This change is illustrated in figure 13.
   (b) The periodic point x_α on S undergoes a period-doubling or a Hopf bifurcation, if $n \geq 3$, thereby changes its stability. See sub-subsection 2.2.1 for these bifurcations.
2. The periodic point x_α on S undergoes a homoclinic tangency bifurcation. This happens mostly in the neighbourhood of tongue boundaries. See sub-subsection 2.2.2 for this bifurcation. In figure 14 (left) is an horseshoe in a map with homoclinic points.

[3] See Broer, Simó and Tatjer [7] §2.2 for a mathematical definition.
[4] For more information about the Horse shoe map, see chapter 2 of B. Braaksma in [9].

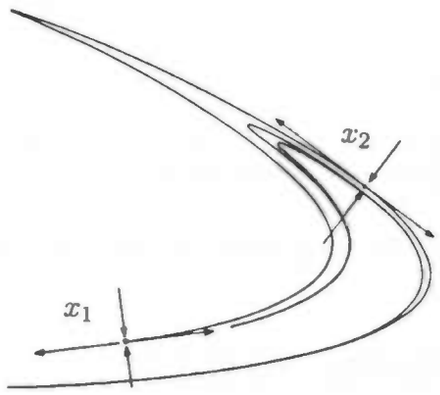

Figure 12: The Hénon attractor is the closure of the unstable manifold of one of his saddle points. $H = \overline{W^u(x_1)}$, Ruelle [30].

Figure 13: The invariant circle loses normal hyperbolicity, the *node* x_α becomes a *focus*.

Figure 14: Horseshoe in a map with homoclinic points (left); Stable and unstable manifold of x_α (right).

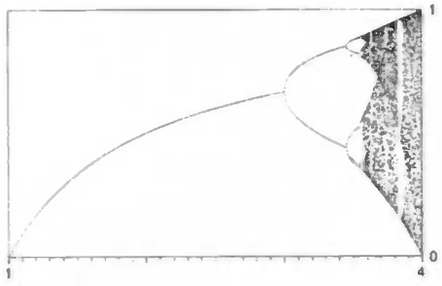

Figure 15: Quadratic map: Limit set diagram, Peitgen et al. [26].

Therefore the stable and unstable manifold of x_a are closely intertwined, see figure 14 (right).

Remarks

1. Tongue boundaries accumulate often at curves of homoclinic tangency bifurcations. Therefore chaotic attractors are expected for parameter values where tongue boundaries accumulate.

2. When Arnol'd tongues, belonging to the "same" invariant circle, overlap, one may assume that invariant circles are destroyed. At those places chaotic attractors maybe expected.

3. **The Newhouse-Ruelle-Takens scenario (NRT scenario).**
   Let the 3-dimensional (Poincaré) map f have an invariant 2-torus. Furthermore the three frequencies of the corresponding 3-torus in the 4 dimensional vector space have no rational relation. Then small Hénon-like chaotic attractors generically occur on the 2-torus of the Poincaré map. This is a special case of the destruction of an invariant circle by an homoclinic tangency bifurcation. The theorem is stated in Newhouse et al. [24], which is written on basis of the articles of Ruelle and Takens [27, 28]. See also Palis and Takens [25].

2.5.2 Period doubling route to chaos

The period-doubling route of fixed or periodic points to chaos also may occur in the map f_a. This well-known route can appear both outside and inside an Arnol'd tongue. Compare the routes in the quadratic map and the Hénon-map, see Devaney [10] and Peitgen et al. [26]. Figure 15 shows the limit set diagram of the quadratic map. This figure is taken from Peitgen et al. [26].

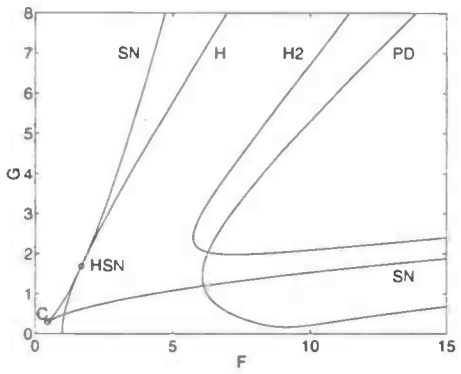

Figure 16: The autonomous Lorenz-84 system: Bifurcation diagram in the (F, G) parameter plane, two Hopf curves (H), (H_2) and saddle-node curve (SN) of fixed points are depicted. H and SN are tangent in Hopf-saddle-node point (HSN) and SN meets a cusp (C). Also the period doubling curve (PD) of the limit cycle is depicted.

3 The autonomous Lorenz-84 system

The driven Lorenz-84 system with ε small is a perturbation of the autonomous Lorenz-84 system, $\varepsilon = 0$. So we first mention the bifurcations of the equilibria in the autonomous system. These results can also be found in the papers of Broer, Homan, Hoveijn and Krauskopf [4], Homan [16], Sicardi Schifino et al. [23] and Shil'nikov et al. [32]. The relation between this 3-dimensional vector field and the corresponding 3-dimensional Poincaré map $f_{\varepsilon=0,\alpha}$ is given in subsection 3.3.

3.1 The equilibria & the limit cycle

A unique equilibrium, $(X, Y, Z) = (F, 0, 0)$, exists for parameter values $(F, G) = (F, 0)$. This solution is denoted by O_1. O_1 is stable for $\{(F, G)$: $0 < F \leq 1$, $G = 0\}$. For G (relatively) large O_1 is the only stationary solution.
O_1 undergoes a super-critical Hopf bifurcation at $(F, G) = (1, 0)$ it becomes unstable and a stable limit cycle appears. The numerical continuation of this Hopf bifurcation, H, in the (F, G)-plane is shown in figure 16. This curve can also be derived analytically, see Shil'nikov et al. [32].
Also a curve of saddle node bifurcations (SN) is continued in the parameter plane, see figure 16. At one side of the curve there is one equilibrium and at the other side are three. Furhermore another curve of Hopf bifurcations (H_2) exists in the (F, G)-plane. When crossing this curve as F_0 increases a stable equilibrium becomes unstable and a stable limit cycle appears. This bifurcation curve is discussed in Sicardi Schifino et al. [23].
There are two codimension 2 points on the codimension 1 curves, the SN curve meets a cusp bifurcation (C) and the SN curve is tangent to the H curve at a Hopf saddle-node bifurcation (HSN). The Hopf bifurcation becomes subcritical above this bifurcation point and the system for nearby parameter values may give rise to very rich dynamical behaviour which may extend far away. For instance a Neimark-Sacker bifurcation [5] curve emerges from the HSN point.

[5] At a Neimark-Sacker biurcation a limit cycle undergoes a "Hopf" bifurcation resulting in a 2-torus with

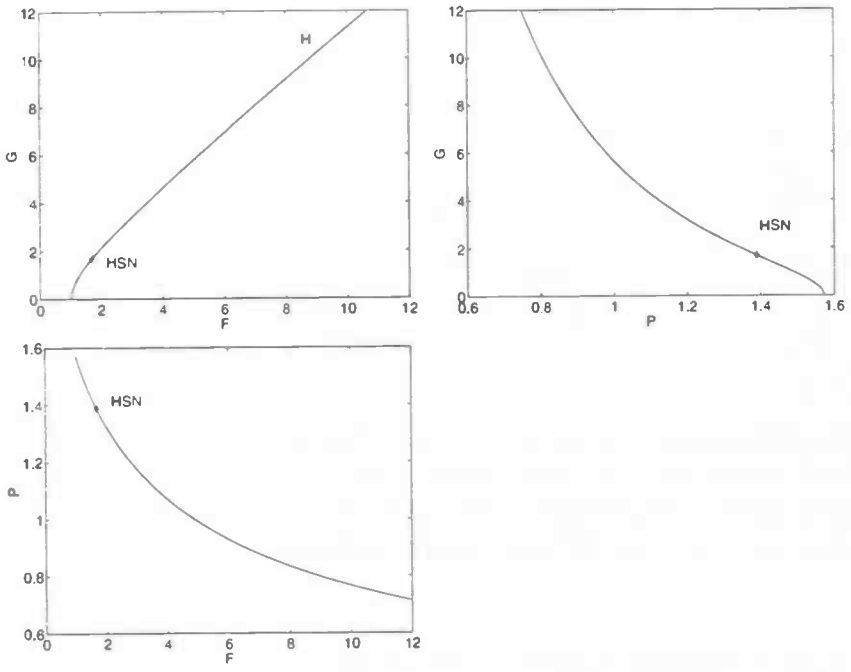

Figure 17: Lorenz-84: Hopf curve (H) in (F, G) parameter plane, period $P_{(F,G)}$ along H is given by plotting F versus $P_{(F,G)}$ and G versus $P_{(F,G)}$.

And an invariant 2D torus exists in a part the (F, G)-plane. Also limit cycles of long period existing near a curve of homoclinic bifurcations are found. See for more information and figures Broer, Homan, Hoveijn and Krauskopf [4], Homan [16] and Shil'nikov et al. [32]. The limit cycle that exists at the right of the curve of Hopf bifurcations (H) undergoes a period doubling bifurcation (PD). This bifurcation is also continued in the parameter plane, curve PD, see figure 16.

3.2 Period of the limit cycle

The period of the limit cycle occuring at the right hand side of the H curve varies along this curve. The period $P_{(F,G)}$ of the limit cycle at parameter values (F, G) is determined with AUTO [11]. The period is maximal at $(F, G) = (1, 0)$, $P_{(1,0)} \approx 1.5708$ and decreases monotonically, $P_{(11.3,12.7)} \approx 0.7300$. At the HSN point where the Hopf bifurcation switches from supercritical to subcritical, $P_{(1.684,1.683)} \approx 1.389$. In figure 17 the Hopf curve (H) is depicted in the (F, G) parameter plane and the period $P_{(F,G)}$ along H is plotted versus F and G.
The period is used to determine the rotation number $\rho = \frac{T}{P}$ of the invariant circle of the map $f_{\varepsilon,\alpha}$ corresponding to the driven Lorenz-84 system, see the remark in subsection 2.3 and section 4. At points on the Hopf curve, where this quotient is rational, Arnol'd tongues will emerge, see subsection 2.4.

either periodic or quasi-periodic behaviour, see Guckenheimer and Holmes [13] and Kuznetsov [19].

3.3 Poincaré map for $\varepsilon = 0$

The Poincaré-map $f_{T,\varepsilon=0,\alpha}$ is the time T map of the autonomous Lorenz-84 system. (For simplicity $f_{T,\varepsilon=0,\alpha}$ will be denoted as f_α in this subsection.) The fixed points x_α of f_α are trivial period T-solutions corresponding to the equilibria of this autonomous system. Let A_{x_α} be the matrix corresponding to the linearisation in the equilibrium x at parameter value α.

$$\dot{\zeta} = A_{x_\alpha}\zeta + O|\zeta^2|$$

The stability of x_α is determined by the eigenvalues λ_i of the matrix A. The stability of the corresponding fixed point of map f_α is investigated by looking at eigenvalues μ_i of the linearisation of the map f_α around this fixed point: $D_{x_\alpha f_\alpha}$. Since f_α is just the T-flow of the autonomous system the following equation holds:

$$D_{x_\alpha f_\alpha} = e^{TA_{x_\alpha}}$$

So there is a connection between the eigenvalues of the linearized map and the linearized vector field:

$$\mu_i = e^{\lambda_i}$$

for example if the equilibrium x_α undergoes a Hopf bifurcation then x_α has eigenvalues $\mu_{1,2} = \pm i\omega$. This means that the corresponding fixed point x_α also undergoes a Hopf bifurcation (for maps) at the same parameter value. The fixed point x_α has eigenvalues $\lambda_{1,2} = e^{\pm i\omega}$. This bifurcation generates a closed invariant circle S. However the Hopf bifurcation of the fixed point is degenerate and there will be no frequency locking on the invariant circle S. This is obvious because the system is independent of the period of the forcing T. At the right hand side of the Hopf curve there are only tongue hairs, lines in the parameter plane, with parallel dynamics on S.

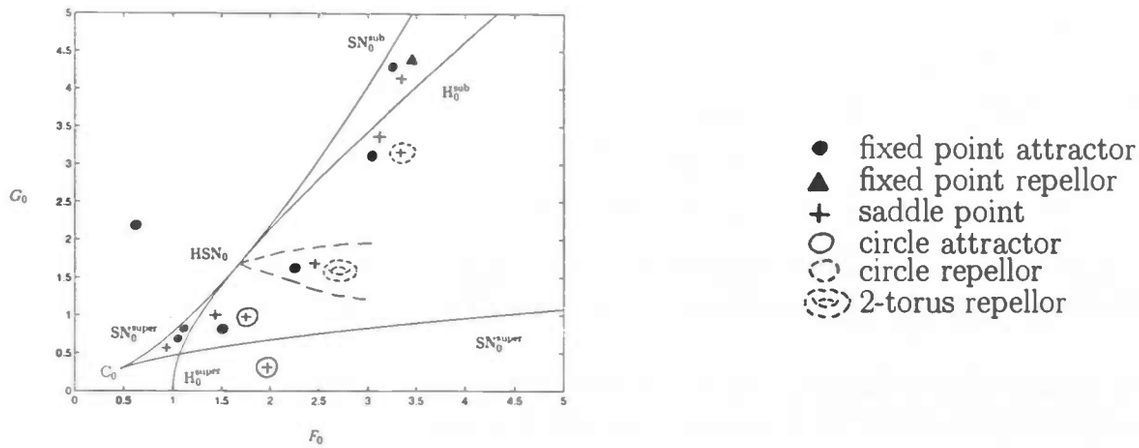

Figure 18: Driven Lorenz-84 system for $\varepsilon = 0$: Framework of codimension 2 bifurcation points and codimension 1 bifurcation curves of the fixed points of the map $f_{0,\alpha}$ in the (F_0, G_0)-plane. In each region fixed points, invariant circles and invariant tori are indicated.

4 Generic expectations for driven Lorenz-84

Section 3 provides us with some a framework of bifurcation curves and bifurcation points in the (F, G)-plane of the autonomous Lorenz-84 system, see figure 18 for a sketch. On basis of these results we give theoretical expectations for the Poincaré-map $f_{\varepsilon,\alpha}$ of driven Lorenz-84 with $0 < \varepsilon \ll 1$, assuming that the map $f_{\varepsilon,\alpha}$ is a generic perturbation of the degenerate map $f_{0,\alpha}$.
From the theory of dynamical systems it follows that the following features of the map $f_{0,\alpha}$ corresponding to Lorenz-84 are persistent. Main argument for the persistence are *hyperbolicity* and *normal hyperbolicity*, compare also Broer et al. [6], section 2.

1. The hyperbolic fixed points.
2. The saddle-node curve (SN) .
3. The Hopf curve (H).
4. The Hopf-saddle-node point (HSN) and the cusp.
5. The invariant circle near the Hopf curve.
6. The invariant 2-torus at the right of the HSN point.

Main difference and of most interest is that by assumption the bifurcations of fixed points in the map $f_{\varepsilon,\alpha}$, $\varepsilon \neq 0$ in general will not be degenerate.
Thus for ε small we expect a curve of Hopf bifurcations in the (F_0, G_0)-plane not far from the curve H_0. Again there is a HSN point on this curve but now for maps. Below this point the bifurcation is supercritical thus an attracting invariant circle appears upon crossing the Hopf curve for fixed G_0 and increasing F_0. Above this point the bifurcation is sub-critical thus a repelling invariant circle appears upon crossing the Hopf curve for fixed G_0 and increasing F_0. At the right-hand side of the H_ε curve we expect that the parameter plane is structured

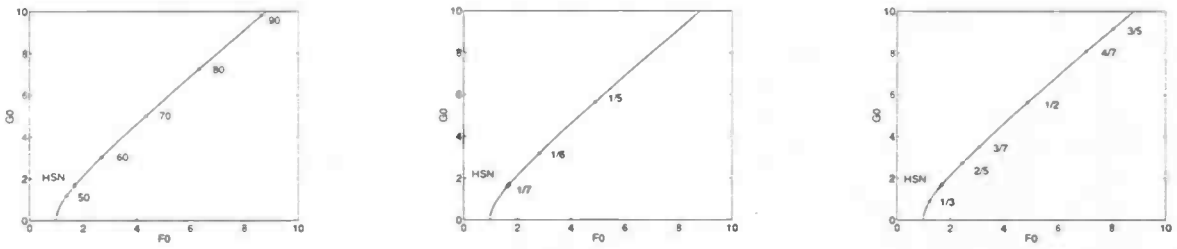

Figure 19: Driven Lorenz-84 system with $\varepsilon = 0$ and respectively $T = 73$, $T = 0.2$ and $T = 0.5$: H_0 curve with the rotation number of the invariant circle existing at the right of H_0.

by Arnol'd tongues emerging from H_ε at points where the rotation number ρ is rational, see subsection 2.4. Inside the tongues there will be frequency locking on the invariant circle, S. And outside the tongues there will be quasi-periodic dynamics on S.
At further distance of H_ε the invariant circle may lose its smoothness due to the change of stability of periodic points on the invariant circle or due to an homoclinic tangency bifurcation, see subsection 2.5. Also Arnol'd tongues with different rotation number may overlap at further distance of H_ε. Then the invariant circle probably will be destroyed, see remark 2 in sub-subsection 2.5.1.
Furthermore at the right hand side of the HSN_ε point we expect an area in the (F_0, G_0)-plane where a repelling invariant 2-torus of the map $f_{\varepsilon,\alpha}$ exists. On such 2-tori chaotic dynamics may occur (NRT scenario), see remark 3 in sub-subsection 2.5.1.
On basis of these expectations numerical investigations are made for the driven Lorenz-84 system with periods $T = 73$, $T = 0.2$ and $T = 0.5$. We mainly search for Arnol'd tongues with a large rotation number $\rho = \frac{p}{5}$. To locate these the rotation number ρ along the Hopf curve is determined for the different values of T, see figure 19. The estimation $\rho = \frac{T}{P_{(F,G)}}$ with $P_{(F,G)}$ the period of the limit cycle appearing at the Hopf curve (H) in the autonomous Lorenz-84 system is used. $P_{(F,G)}$ is determined with AUTO [11], see subsection 3.2.
In the case $T = 73$ the period of forcing is large compared to the period of the limit cycle, that appears at the right hand side of the Hopf curve in the autonomous Lorenz-84 system. So the rotation number is large and varies quickly along the Hopf curve, see figure 19. Indeed, the rotation number varies between 46.52 and 52.55 along the part of the Hopf curve between the F_0-axis and the HSN point. So the Hopf curve will meet a lot of strong resonance points. At such codimension 2 bifurcations the Hopf curve is destroyed and curves of homoclinic bifurcations are expected to emerge. This complicates the bifurcation diagram considerably. for example six occurrences of the BT bifurcation are expected on the super-critical part of the Hopf curve, namely for $\rho = 47, 48, \cdots, 51$ or 52, see sub-subsection 2.2.1 for this bifurcation. Furthermore in a part of the Hopf curve where the rotation number varies from $\tilde{\rho}$ to $\tilde{\rho} + 1$ all sort of tongues can be expected to emerge, see subsections 2.3 and 2.4. These tongues are probably very thin since ρ varies rapidly.
The results of the numerical investigations of the actual driven Lorenz-84 system are presented in the next three sections.

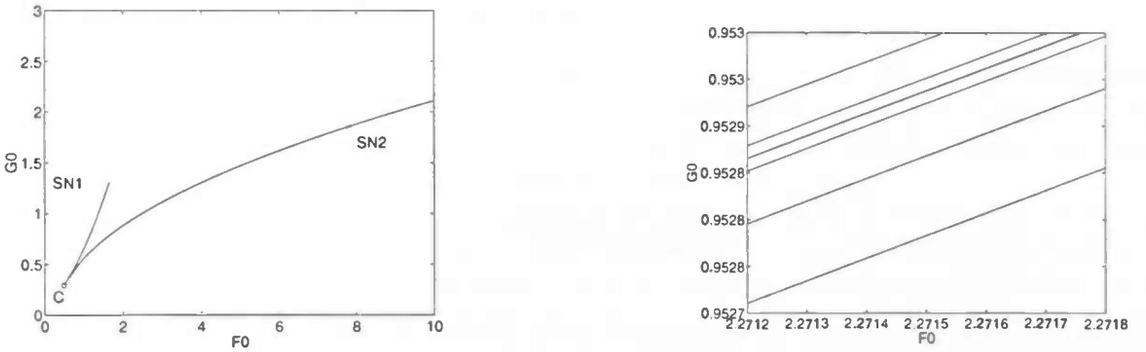

Figure 20: Driven Lorenz-84 system with $T = 73$ and $\epsilon = 0.5$: Bifurcation diagram in the (F_0, G_0)-plane, the saddle-node curves SN_1 and SN_2 colliding in cusp C (left) and a magnification of the SN_2 region (right).

5 The driven Lorenz-84 system with year rhythm

The period $T = 73$ corresponds to the year rhythm. This is the most realistic period because the system simulates the seasonal period. The period is large compared to the characteristic periods of the autonomous system. When investigating this system some "numerical" problems occur in AUTO [11] and DsTool [14]. To get a next iterate of the Poincaré map for $T = 73$ many integration steps have to be taken and numerical errors can play a significant role in the solution. Runge-Kutta 4, the standard integration routine of DsTool, [14] turns out to be not accurate enough for this. C. Simó also investigated the driven Lorenz-84 system with year rhythm with self-made software which uses a, in this case, more accurate integration routine. An advantage of self-made software is that all sort of defaults, like for example precision and output-structure, easily can be changed if necessary. The results, C. Simo obtained, are discussed in subsection 5.2.

5.1 The bifurcations of the fixed points

In this subsection the results are given of the investigation of the driven Lorenz-84 system with $\epsilon = 0.5$. Only this value is considered because with AUTO [11] no qualitative different results at other values of ϵ are found.
In figure 20 (left) parts are presented of the saddle node curves SN_1 and SN_2 of fixed points of the driven system with $T = 73$ and $\epsilon = 0.5$. SN_1 and SN_2 collide in cusp C. These curves correspond to the SN curve with its cusp (C) of the autonomous system. SN_2 meets many other cusp bifurcations and goes the other way around very near it came from, see 20 (right) for a magnification at this region.
For (F_0, G_0)-values at the left side of the SN_1 curve or below the SN_2 curve one fixed point exists. And for (F_0, G_0)-values at the right side of the SN_1 curve and above the SN_2 curve three fixed points exist as to be expected near the cusp C, compare sub-subsection 2.2.1. However a lot of fixed points where detected in a thin area around the SN_2 curve. How many fixed points exist is not known since in the continuation of the fixed points around the SN_2 curve convergence problems occur.
Remark

1. The infinite number of saddle node bifurcations can point to a *Shil'nikov bifurcation* in

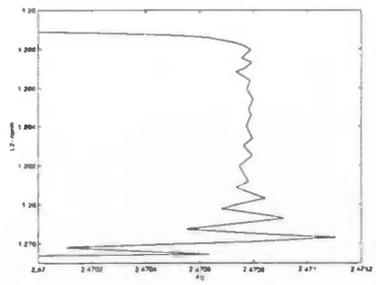

Figure 21: Driven Lorenz-84 system with $T = 73$, $\varepsilon = 0.5$, $G = 1$, and varying F_0: overview of the SN bifurcations of the limit cycle around $F_0 = 2.4708$, the L2-norm of the coordinates plotted against F_0.

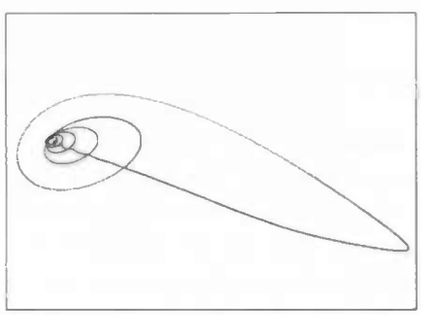

Figure 22: Driven Lorenz-84 system with $T = 73$, $\varepsilon = 0.5$ and $(F_0, G_0) = (2.4708, 1)$: projection onto the (X, Y)-plane of a stable limit cycle in the neighbourhood of a Shil'nikov bifurcation.

the corresponding 4 dimensional vector field. The *Shil'nikov bifurcation* is a homoclinic bifurcation of an equilibrium in an (at least 3 dimensional) vector field that generates an infinite number of limit cycles several of which have large periods. For theory about the Shil'nikov bifurcation, see Glendinning and Sparrow [12] and Kuznetsov [19]. Figure 21 shows the results of the continuation of the limit cycle detected at the left side of SN_1 by varying F_0 and taking $G_0 = 1$ fixed. Around $F_0 = 2.4708$ the limit cycle undergoes many saddle node bifurcations, creating many different limit cycles. Also period doubling bifurcations are detected round these parameter values. Figure 22 shows the projection onto the (X, Y)-plane of a stable limit cycle at $(F, G) = (2.4708, 1)$. This cycle looks like a limit cycle in the neighbourhood of a Shil'nikov bifurcation. Both figures strengthen the thought of the existence of a curve of Shil'nikov bifurcations in the SN_2 region.

2. A homoclinic bifurcation in the 4 dimensional system gives rise to a homoclinic tangency bifurcation in the corresponding map $f_{\varepsilon,\alpha}$.

For $\varepsilon = 0.5$ the stable fixed point undergoes a super-critical Hopf bifurcation in the neighbourhood of $(F_0, G_0) = (1, 0)$. Due to a bug in `AUTO` [11] the Hopf bifurcation curve in the (F_0, G_0)-plane could not be determined. We neither succeed in detecting frequency locking with `DsTool` [14].

5.2 Numerical results by C. Simó

In this subsection some results are presented obtained by C. Simó. He used as integration routine a Taylor expansion up to order 24. In this case this routine gives more accurate results than the Runge-Kutta 4 routine of `DsTool` [14]. Furthermore the software is in a way that limit sets at many different parameter values are determined at once.
The driven Lorenz-84 system is investigated for the realistic values $T = 73$ and $\varepsilon = 0.5$. For many (F_0, G_0)-values the stable limit set or attractor of the orbit starting at $(X_0, Y_0, Z_0) = (3, 2, 1)$ is determined so there can be no detection of coexistence of attractors. The limit set is on an invariant circle for parameter values (F_0, G_0) at the right-hand side of the expected Hopf curve (H) with G_0 small. On these invariant circles both periodic orbits with all sort of periods corresponding to different Arnol'd tongues and quasi-periodic behaviour corresponding to areas between these tongues are observed. For larger values of G_0 also chaotic limit sets are detected. And the behaviour becomes simple again for G_0 sufficiently large.
As an example we look at Y-values of the limit set of $F_0 = 9$ for increasing value of G_0, see figure 23 for a kind of limit set diagram, its construction is explained in the below standing remark. Furthermore in figure 24 projections are shown onto the (Y, Z)-plane for several values of G_0. We now recapitulate in words what happens.
For G_0 small an invariant circle exists, denoted by S, see figure 24-(1). S doubles in a (quasi-periodic) period doubling bifurcation around $G_0 = 0.37$, see the remark in sub-subsection 2.2.1. Then it loses its stability thereby creating a circle attractor, denoted by $2S$, of double length and roughly half the rotation number, see figure 24-(2). This bifurcation corresponds with the first period doubling bifurcation of the limit cycle in the autonomous system, see the PD curve in figure 16.
What then happens is the following. The unstable manifold W^u(S) of S is attracted by $2S$. (Also compare the 'whirlpool' phenomenon as described by Shil'nikov et al. [32].) In turn, around $G_0 = 0.6$, the doubled curve $2S$ loses stability again and the unstable manifold create strange attractors by folding, see figures 24-(3)-(5). Compare with the Hénon attractor being created by folding of the unstable manifold of a saddle-point, see figure 12. In the chaotic region also parameters exist where periodic dynamics is found, for example a period 3 attractor at $G_0 = 0.68$, see figure 24-(4). For $G_0 = 1.96$ the limit set is a chaotic attractor, see figure 24-(6). But for $G_0 = 1.97$ the limit set has become a fixed point, see figure 24-(7). What sort of (inverted) route to chaos appears here will be investigated by Broer and Simó, see [8]. Around $G_0 = 2.21$ the fixed point undergoes a Hopf bifurcation and an invariant circle reappears, also on this circle tracks of periodic behaviour are found, see figure 24-(8). Finally around $G_0 = 5.76$ this invariant circle disappears in an inverted Hopf bifurcation and a fixed point reappears. These two Hopf bifurcations correspond with the Hopf bifurcation, H_2, of equilibria in the autonomous system, see the H_2 curve in figure 16.
For small values of $|\varepsilon|$ the familiar alteration of periodicity and quasi-periodicity is suggested by figure 23. Indeed, the windows seem to be associated to Arnol'd tongues. However the windows are partly an artifact of the construction. In the next remark we explain the construction of the limit set diagram of figure 23.
Remark

1. The limit set diagram in figure 23 is not a regular one like for example the limit set diagram in figure 12. It provides only a rough overview. The diagram is constructed as follows.
   The parameter $F_0 = 9$ is fixed and G_0 varies along the horizontal axis. In the diagram

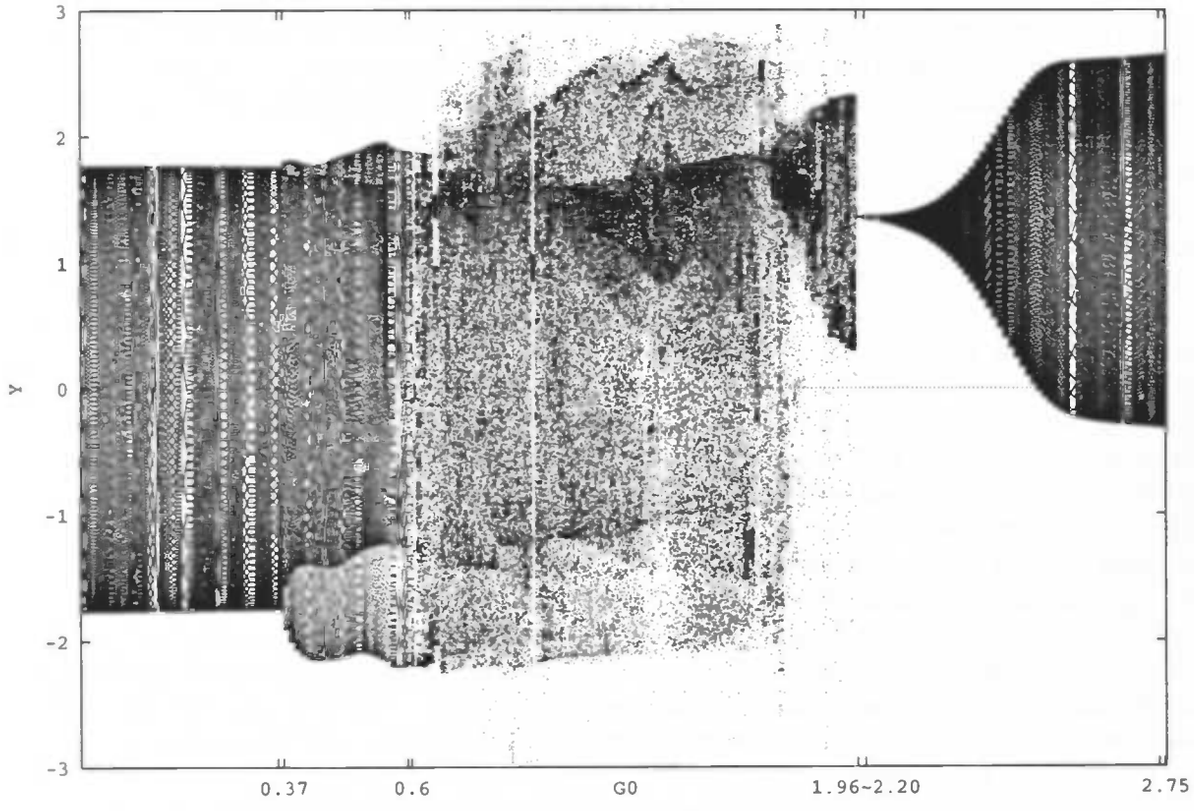

Figure 23: Driven Lorenz-84 system with $T = 73$ and $\epsilon = 0.5$: Limit set diagram, taking $F_0 = 9$ fixed and G_0 varying from 0.01 to 2.75. G_0 does not increase evenly, see remark 1.

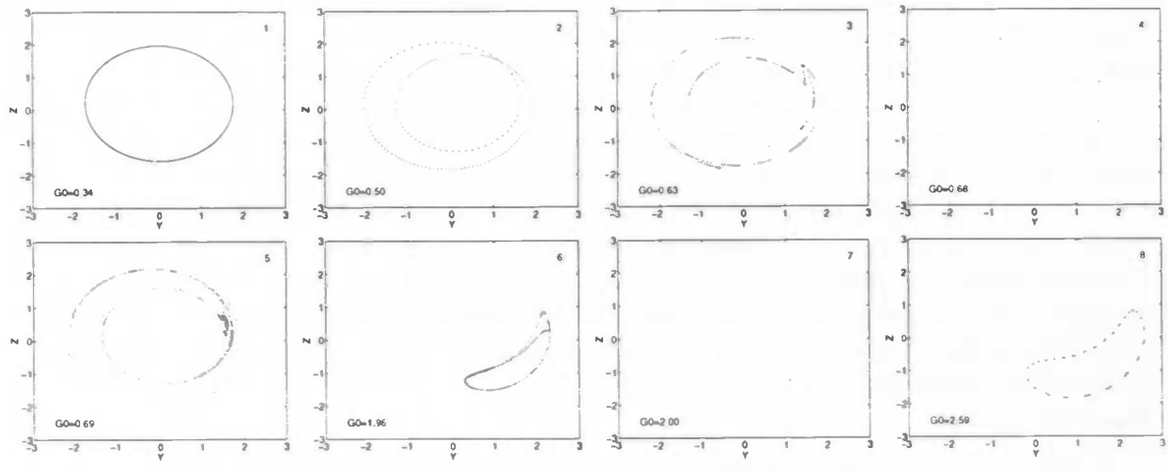

Figure 24: Driven Lorenz-84 system with $T = 73$, $\epsilon = 0.5$ and $F_0 = 9$: attractors for different values of G_0.

G_0 starts at 0.01 and increases with steps of size 0.01 to 2.75. For each pair (F_0, G_0) the orbit starting in $(X_0, Y_0, Z_0) = (3, 2, 1)$ is determined. To create "limit" sets the first (transient) part of the orbit, about 2000 points, is not printed. In the diagram each value of G_0 is represented by a small bar. In a bar the (different) Y values of points of a limit set are put one after the other. The bars have not the same width everywhere. The limit set consists of 2000 points when the set is quasi-periodic or chaotic. See for example the bar in the case $G_0 = 0.37$. But the limit set consists of much less than 2000 points when the set is periodic. for example in the interval $1.96 < G_0 < 2.21$ the limit set is a fixed point. The limit sets of these cases are represented by just as many points as those at one value of G_0 in a quasi-periodic or chaotic case. Consequently stationary and periodic behaviour are hardly seen in the diagram, although this occurs often.

5.3 Conclusion

We conclude that the bifurcation diagram of the Lorenz-84 system with year rhythm is complicated and interesting , although hard to investigate with `AUTO` [11] and `DsTool` [14]. As we saw, one reason is that the period $T = 73$ is very large compared to the characteristic periods of the autonomous system. C. Simó obtains better results by using self-made software. An advantage of self-made software is that all sort of defaults, like for example integration routine with its precision and output-structure, easily can be changed if necessary. The Taylor expansion routine up to order 24) is used. This routine is more accurate in the case $T = 73$ than Runge-Kutta 4. The results obtained by C. Simó give a clear indication for the existence of Arnol'd tongues.

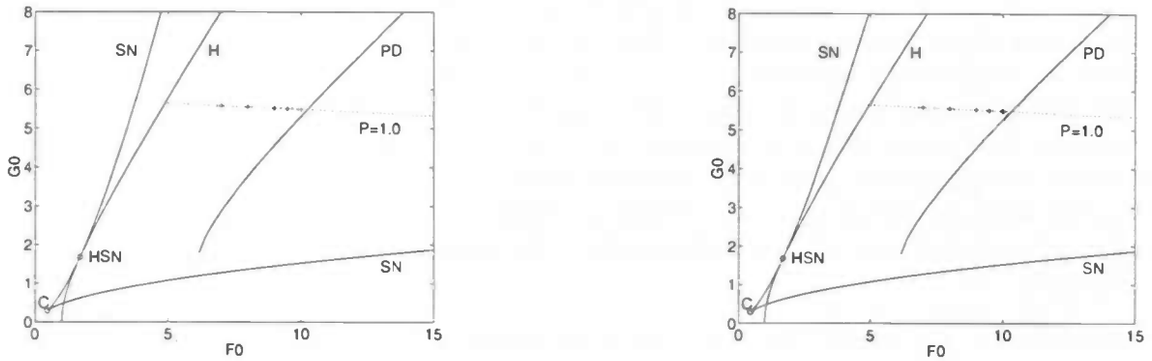

Figure 25: Driven Lorenz-84 system with $T = 0.2$ and $\varepsilon = 0.1$ (left), $\varepsilon = 1.0$ (right): Bifurcation diagram in the (F_0, G_0)-plane consisting of the saddle-node curve (SN) meeting a cusp (C) and the Hopf curve (H) of fixed points which is tangent to SN in the HSN point, the (quasi-periodic) period-doubling curve (PD) of the invariant circle, the curve of the autonomous Lorenz-84 system where $P_{(F,G)} = 1.0$ and the upper and lower boundary of the 1:5 resonance tongue (+), the boundaries are so close that you only see one + for one value of F_0.

6 The driven Lorenz-84 system with day rhythm

The Lorenz-84 system is actually a climate system with mainly large-scale effects, both in space and in time. It is also interesting to know whether short time disturbances influence the system or not. So we choose to simulate the day-night cycle and take the forcing period $T = 0.2$. At this T, the system does not have to be integrated that long to get the next iteration of the Poincaré map, so more accurate results are obtained by `AUTO` [11] and `DsTool` [14].

6.1 The bifurcations of the fixed points

The saddle-node curve (SN) and the Hopf curve (H) of fixed points for $0 < \varepsilon \leq 1$ only gradually are perturbed away from the corresponding curves in the autonomous case. Compare the bifurcation diagrams in the cases $\varepsilon = 0.1$ and $\varepsilon = 1$, in figure 25, with the diagram of the autonomous system, in figure 16.

For all ε the SN curve and the H curve remain tangent at the HSN point and the SN curve meets a cusp point (C). The rotation number ρ varies slowly along the H curve, see figure 19 in section 4. The rotation number of the circle attractor varies between $0.127 < \rho < 0.144$. The rational numbers with the smallest denominators in this interval are $\frac{1}{7} \approx 0.143$ and $\frac{2}{15} \approx 0.133$. At the right side of these points you would expect areas (tongues) where respectively a period 7 attractor and a period 15 attractor exist on the circle attractor. But only quasi-periodic behaviour is seen, even at a quite large distance of the H curve. Probably the Arnol'd tongues remain thin.

The tongue belonging to the rational rotation number with denominator 5 is expected to be the widest, see subsection 2.4. Hence we look at the place where $\rho = \frac{1}{5}$ is expected for ε small. That is where a limit cycle exists with $P = 1.0$ in the autonomous system. The curve in the (F_0, G_0)-plane where a limit cycle exists with period $P = 1.0$ is given in figure 25. We searched for a period 5 repellor on the circle repellor of the driven Lorenz-84 system in the

neighbourhood of this curve with successively $\varepsilon = 0.1$, 0.5, 1.0, 2.0, 4.0 and 7.0. Particularly we looked at parameter values just before the limit cycle undergoes a PD bifurcation, since here the tongues are expected to be the widest. Another example of this phenomenon is the fattened Arnol'd map, see Broer, Simó and Tatjer [7]. However DsTool [14] experiments indicate the tongue with $\rho = \frac{1}{5}$ is still very thin, if it exists at all. For $0 < \varepsilon \leq 7$ no open area in the parameter plane with frequency locking is found. It is expected that tongues will be wider for increasing ε and increasing distance to the H curve. To check this for the Arnol'd tongue with $\rho = \frac{1}{5}$ practical boundaries are determined. This is done by the following criterion:

Criterion 1 *The upper respectively the lower boundary of a tongue is the largest value respectively the smallest value of G_0 at fixed F_0 where the invariant circle of the Poincaré-map is not filled after 10000 iterates.*

The results of the investigation are surprising. The distance between the boundaries appear to be 0.006 ± 0.001, independent of the distance to the Hopf curve or the size of ε, varying from 0 to 7. For $\varepsilon = 0.1$ and $\varepsilon = 1$ this practical boundaries are in the bifurcation diagram of figure 25 respectively (left) and (right). If there is an Arnol'd tongue with $\rho = \frac{1}{5}$ then it is not wider than 0.001 up to $\varepsilon \leq 7$.
Further exploration with DsTool [14] of the map $f_{\varepsilon,\alpha}$ with $0 < \varepsilon < 1$, for example around the HSN point, and the point $(F_0, G_0) = (7, 1)$, which is in the meteorological interesting area, gives the same attractors and repellors as the map $f_{0,\alpha}$.

6.2 Conclusion

We conclude that with DsTool [14] and AUTO [11] no qualitative differences are detected between the maps $f_{\varepsilon,\alpha}$ for $0 < \varepsilon \leq 1$ of the driven Lorenz-84 system with $T = 0.2$ and the degenerated map $f_{0,\alpha}$. Therefore, with these tools no influence of day rhythm on the Lorenz-84 system is detected.

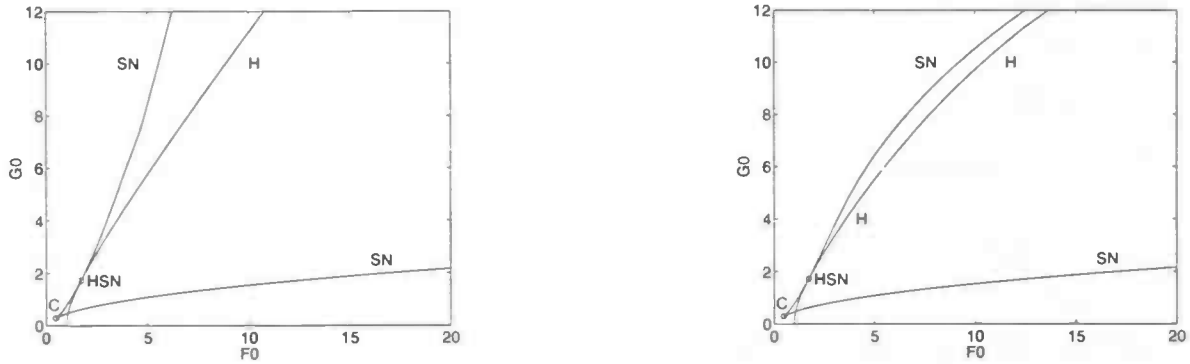

Figure 26: Driven Lorenz-84 with $T = 0.5$ and $\varepsilon = 0.1$ (left) respectively $\varepsilon = 0.5$ (right): Bifurcation diagram of the fixed points in the (F_0, G_0)-plane consisting of the Hopf curve (H), the saddle node curves (SN), the Hopf-saddle-node point (HSN) and the cusp (C).

7 The driven Lorenz-84 system with $T = 0.5$

For the most realistic periods $T = 0.2$ and $T = 73$ we did not succeed in finding frequency locking with `DsTool` [14] and `AUTO` [11]. However Arnol'd tongues are detected in this way when the period $T = 0.5$. This period can still be seen as a daily forcing, since the unit of time (5 days) is just an estimation. We concentrate on the Arnol'd tongues with rotation numbers $\rho = \frac{3}{5}$ and $\rho = \frac{4}{7}$, which are chosen because of their large denominators. These tongues are expected to be the widest. Furthermore the tongues are laying close together on the H curve. For example for $\varepsilon = 0.5$ the tongues overlap and chaotic repellors are found, see subsection 7.3. In subsection 7.2 we treat the development of the Arnol'd tongue with $\rho = \frac{3}{5}$, as ε varies from $\varepsilon = 0.1$ to $\varepsilon = 0.5$, and it turns out that we can divide the tongue structures in several groups. The transitions between the groups are caused by a singularities of the saddle-node surface or codimension 3 bifurcations. These singularities and bifurcations are also discussed in subsection 7.2. Finally in subsection 7.3 some routes to chaos are presented, detected in and around Arnol'd tongues.

7.1 The bifurcations of the fixed points

In this subsection the bifurcation diagrams of the fixed points of the map $f_{\varepsilon,\alpha}$ with $\varepsilon = 0.1$ and $\varepsilon = 0.5$ in the (F_0, G_0)-plane are presented. The diagram in the case of $\varepsilon = 0.5$ shows already the influence of forcing, see figure 26 (right). For example the upper SN curve is bent down to the H curve. This is in contrast with the bifurcation curves of the fixed point in map $f_{\varepsilon,\alpha}$ with day rhythm, see figure 25 in subsection 6.1.
Furthermore the H_ε curve with $\varepsilon = 0.5$ is destroyed around $(F_0, G_0) = (5.4, 5.9)$ due to an 1:2 strong resonance point. Around such a point a complicated bifurcation diagram is expected with also heteroclinic (tangency) bifurcations. An indication for this complicated diagram is given by the strange round at the end of the lower part of H_ε. See figure 27 (left) for a magnification of the strange round. In figure 27 (right) shows an example of a chaotic repellor caused by the 1:2 strong resonance. Interesting (numerical) research remains to be done at this point.

Remark

1. It is surprising that the H curve for $\varepsilon = 0.1$ is not destroyed when $\rho = \frac{1}{2}$. Probably the

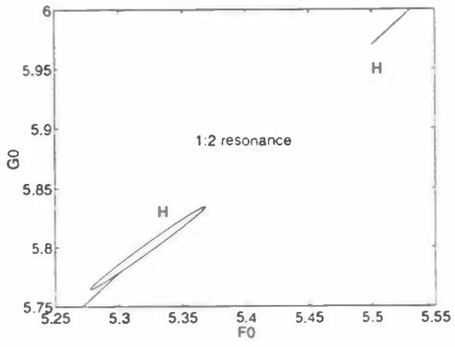

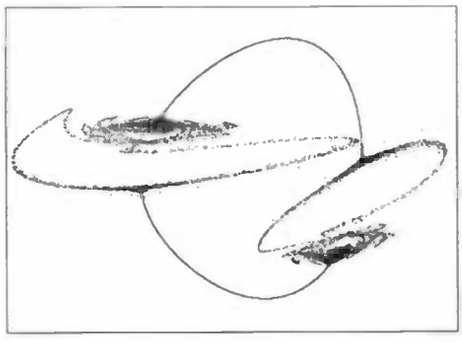

Figure 27: Driven Lorenz-84 system with $T = 0.5$ and $\varepsilon = 0.5$: Magnification of the region where the Hopf curve (H) is destroyed due to a 1:2 strong resonance (left); A chaotic repellor at $(F_0, G_0) = (10, 5.7)$, caused (indirectly) by the 1:2 strong resonance (right).

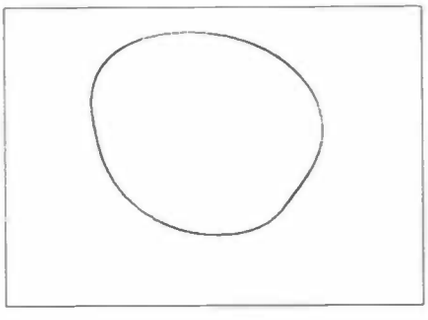

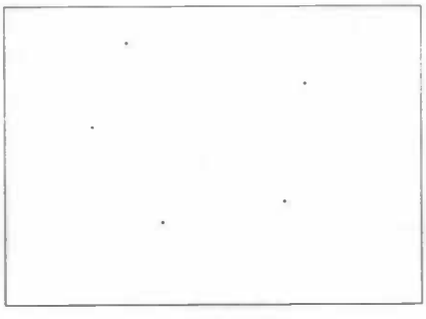

Figure 28: Driven Lorenz-84 system with $T = 0.5$ and $\varepsilon = 0.1$: a quasi-periodic orbit on circle repellor for $(F_0, G_0) = (13, 9.03)$ (left); a period 5 orbit on circle repellor for $(F_0, G_0) = (13, 9.04)$ (right).

step size of the continuation has to be decreased to locate this 1:2 resonance point.

7.2 Arnol'd tongues

In this subsection we discuss the results of the numerical investigation on the Arnol'd tongues with rotation numbers $\rho = \frac{3}{5}$ and $\rho = \frac{4}{7}$. Starting point of the investigation is the rotation number of the map $f_{\varepsilon,\alpha}$ along the Hopf curve, see figure 19 in section 4. We first concentrate at the case $\rho = \frac{3}{5}$. This rotation number occurs on the H curve above the HSN point. So the emanating invariant circle S is unstable and we have to iterate the map $f_{\varepsilon,\alpha}$ backwards to detect a period 5 orbit on S.
Iterating the map $f_{\varepsilon,\alpha}$ backwards with $\varepsilon = 0.1$ and $(F_0, G_0) = (13, 9.03)$ yields a closed invariant circle apparently filled by a quasi-periodic orbit, see figure 28 (left). However taking $\varepsilon = 0.1$ and $(F_0, G_0) = (13, 9.04)$ results in a period 5 repellor, see figure 28 (right).
The parameter values, $\varepsilon = 0.1$, $(F_0, G_0) = (13, 9.04)$ belong to the Arnol'd tongue with $\rho = \frac{3}{5}$. At those parameter values also an unstable period 5 orbit of saddle points is to be expected.

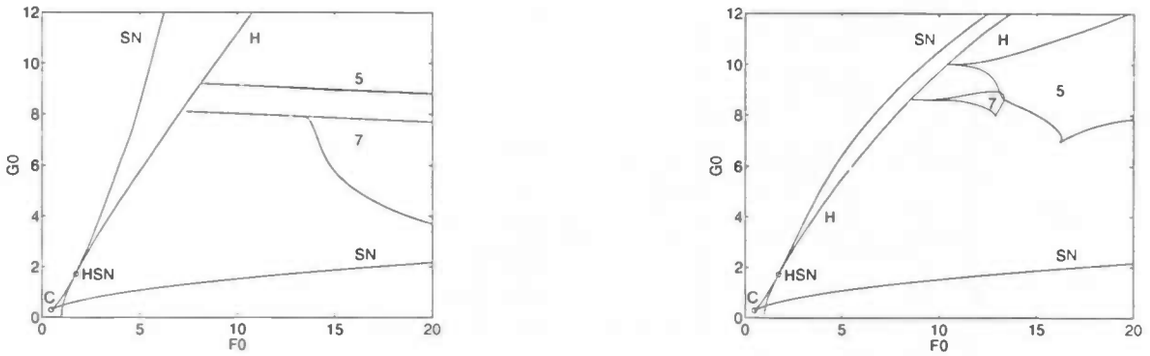

Figure 29: Driven Lorenz-84 system with $T = 0.5$ and $\varepsilon = 0.1$ (left) respectively $\varepsilon = 0.5$ (right): Arnol'd tongues with rotation numbers $\rho = \frac{3}{5}$ (5) and $\rho = \frac{4}{7}$ (7) in the (F_0, G_0)-plane.

However, this orbit is not found since saddle orbits are hard to detect by numerical simulations. The period 5 orbits are located on the unstable invariant circle S which is composed of the stable manifolds of the saddle orbit. The fifth iterate $f^{(5)}_{\varepsilon,\alpha}$ therefore has 5 unstable fixed points and 5 saddle points on S. While one increases or decreases the parameter G_0, keeping $F_0 = 13$ and $\varepsilon = 0.1$ fixed, the stable and the unstable fixed points move over S, colliding and disappearing at SN bifurcations at respectively $G_0 = 9.053$ and $G_0 = 9.031$. The continuation of these bifurcation points in the (F_0, G_0)-plane gives two saddle-node bifurcation curves of period 5 orbits, $\mathrm{SN}_1^{(5)}$ and $\mathrm{SN}_2^{(5)}$, see figure 29 (left). Together they form a typical Arnol'd tongue, approaching a point on the Hopf curve where the eigenvalues of the original fixed points are

$$\mu_{1,2} = e^{\pm i 2\pi \frac{3}{5}}.$$

In the same way the Arnol'd tongue with rotation number $\rho = \frac{4}{7}$ is determined, see figure 29 (left). For the (F_0, G_0)-values inside this tongue (at least two) period 7 orbits exist on the circle repellor.
In figure 29 (right) the same tongues in the case of $\varepsilon = 0.5$ are given. The global structure of the tongues differs at the both values of forcing. The transition of the Arnol'd tongue with $\rho = \frac{3}{5}$ from $\varepsilon = 0.1$ to $\varepsilon = 0.5$ is investigated with great precision. The results of this investigation are presented at the end of this subsection.

Remarks

1. The Arnol'd tongues with rotation number $\rho = \frac{2}{5}$ and $\rho = \frac{3}{7}$ are not investigated because we expect disturbing influence of the HSN point with its complicated bifurcation structure.

2. The Arnol'd tongue with $\rho = \frac{3}{5}$ is wider than the tongue with $\rho = \frac{4}{7}$ in the neighbourhood of the H_ε curve. This agrees with the theoretical expectation about the width of the Arnol'd tongues in section 2.4: a tongue is wider when the rotation number has a smaller denominator.

3. The boundaries $\mathrm{SN}_1^{(7)}$ and $\mathrm{SN}_2^{(7)}$ of the Arnol'd tongue with $\rho = \frac{4}{7}$ in the (F_0, G_0)-plane meet each other in a cusp, when $\varepsilon = 0.5$. We will see further on that this also occurs

Name	connections	ε-interval
A	$1 \leftrightarrow 3,\ 2 \leftrightarrow 4$ $5 \leftrightarrow 6,\ 7 \leftrightarrow 8$	$a \leq \varepsilon < a_{AB}$ with $a \in (0, 0.10]$ and $a_{AB} \in (0.18, 0.19]$
B	$1 \leftrightarrow 3,\ 2 \leftrightarrow 6$ $4 \leftrightarrow 5,\ 7 \leftrightarrow 8$	$a_{AB} \leq \varepsilon < a_{BC}$ with $a_{BC} \in (0.26, 0.28]$
C	$1 \leftrightarrow 2,\ 3 \leftrightarrow 6$ $4 \leftrightarrow 5,\ 7 \leftrightarrow 8$	$a_{BC} \leq \varepsilon < a_{CD}$ with $a_{CD} \in (0.3, 0.305]$
D	$1 \leftrightarrow 7,\ 2 \leftrightarrow 8$ $4 \leftrightarrow 5,\ 3 \leftrightarrow 6$	$a_{CD} \leq \varepsilon < a_{DE}$ with $a_{DE} \in (0.37, 0.374]$
E	$1 \leftrightarrow 7,\ 2 \leftrightarrow 6,\ 4 \leftrightarrow 5$ $3 \leftrightarrow 8,\ 9 \leftrightarrow 10$	$a_{DE} \leq \varepsilon < a_{EF}$ with $a_{EF} \in (0.37408, 0.37409]$
F	$1 \leftrightarrow 9,\ 2 \leftrightarrow 6,\ 4 \leftrightarrow 5$ $3 \leftrightarrow 8,\ 7 \leftrightarrow 10$	$a_{EF} \leq \varepsilon < a_{FG}$ with $a_{FG} \in (0.48, 0.5]$
G	$1 \leftrightarrow 9,\ 2 \leftrightarrow 12,\ 4 \leftrightarrow 5$ $3 \leftrightarrow 8,\ 7 \leftrightarrow 10,\ 6 \leftrightarrow 11$	$a_{FG} \leq \varepsilon < b$ with $b \geq 0.5$

Table 1: The global structure of the Arnol'd tongue with $\rho = \frac{3}{5}$

at the boundaries of the Arnol'd tongue with $\rho = \frac{3}{5}$ when $\varepsilon = 0.28$. There it becomes more clear how such a collision of boundaries is possible.

4. Continuation of the tongues from period $T = 0.5$ to $T = 0.2$ is not realistic, since for $T = 0.2$ the tongues with the rotation numbers $\rho = \frac{3}{5}$ and $\rho = \frac{4}{7}$ would emerge from the H curve around $(F_0, G_0) \approx (100, 100)$.

In figure 29 we saw the difference between the global structures of the Arnol'd tongues with $\rho = \frac{3}{5}$ in the cases $\varepsilon = 0.1$ and $\varepsilon = 0.5$. That is why we investigated the tongue boundaries for several values of ε in the (F_0, G_0) region of seize $(8, 20.5) \times (6, 12)$ to find the cause of the difference. It turns out that the global structure of the tongue varies strongly for changing ε. On basis of the investigations we divide the global structures of the Arnol'd tongue with $\rho = \frac{3}{5}$ and $\varepsilon \in [0.1, 0.5]$ into 7 groups. In figure 30 diagrams are given of Arnol'd tongues which are typical for its structure group. Furthermore there are diagrams where the transition from one group to another becomes clear. The transitions are caused by singularities of the SN surface in the (F_0, G_0, ε)-space and several codimension 3 bifurcations. To make a clear representation of the different structures we numbered the "ends" of the $SN^{(5)}$ curves in the diagrams, see figure 30. A structure is represented by pairs of numbers, which indicate which ends of the curves are connected. The different structures are listed in table 1. A $SN^{(5)}$ curve which connects the ends a and b is denoted by SN_{a-b}. Table 1 and figure 30 together give an overview of the development of the Arnol'd tongue with $\rho = \frac{3}{5}$ for increasing ε. Compare Broer, Simó and Tatjer [7] for a similar approach.

The transitions

1. The transition from structure A to B, from structure C to D and from structure E to F is caused by singularities on the saddle-node surface in the (F_0, G_0, ε)-space. In figure 31 a surface in the 3 dimensional space is given , a so called *saddle-surface*, which has the same singularity. This surface is given by the equation $x^2 - y^2 + z = 0$.

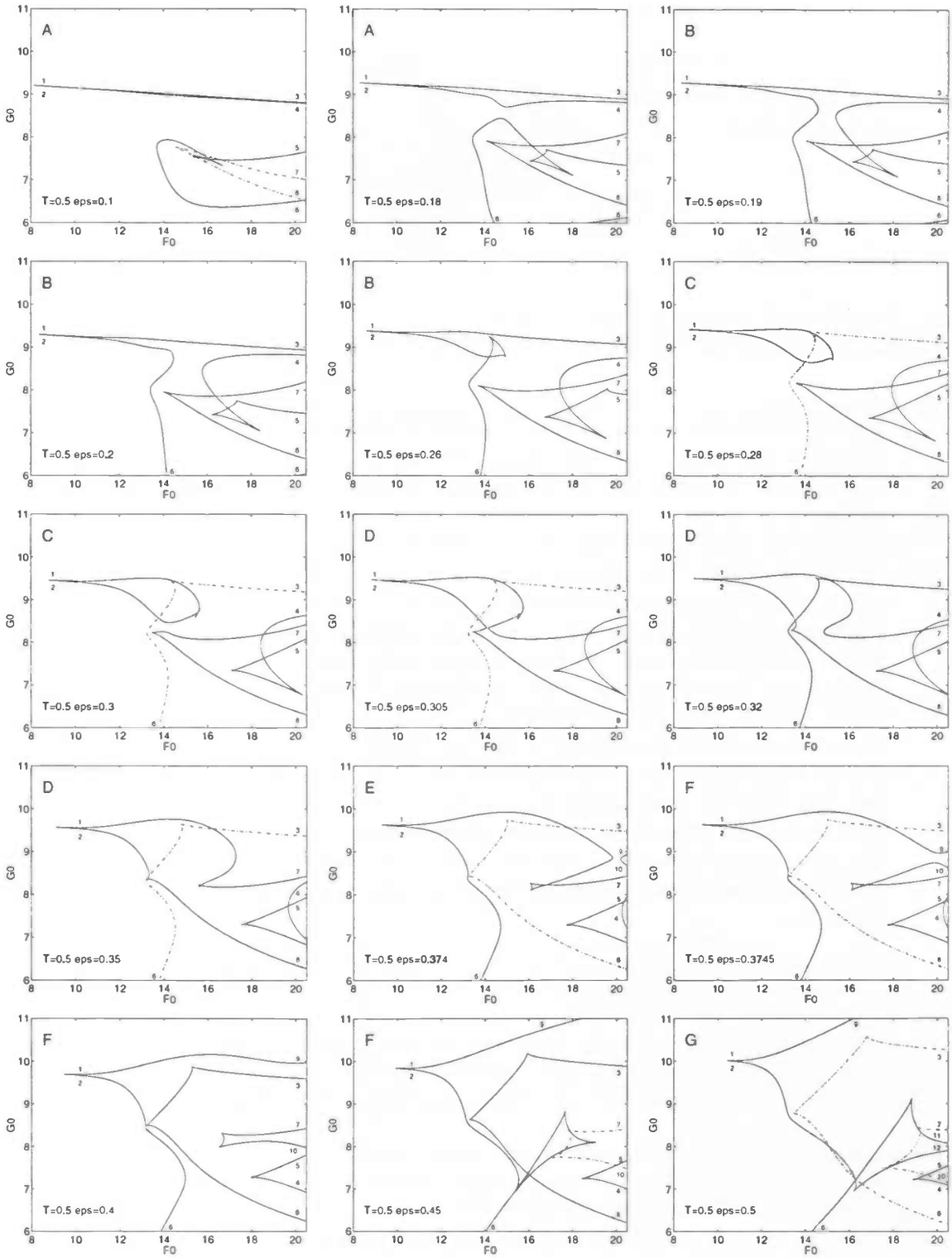

Figure 30: Driven Lorenz-84 system with $T = 0.5$: Diagrams of the global structure of the Arnol'd tongue with $\rho = \frac{3}{5}$ in the (F_0, G_0)-region of seize $(8, 20.5) \times (6, 11)$ for different values of ε. In each diagram the structure is indicated in the upper left corner and the value of ε is put in the lower left corner.

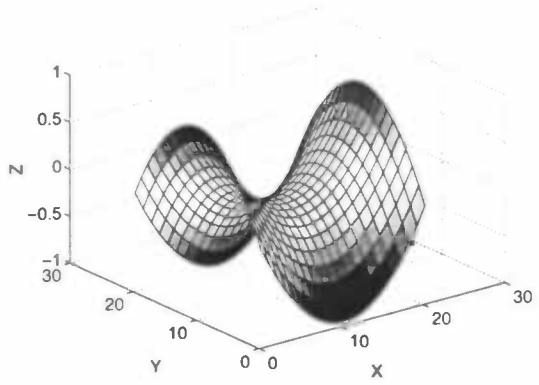

Figure 31: Saddle surface in the 3 dimensional space, given by the equation $x^2 - y^2 + z = 0$

2. The transition from structure B to structure C and from structure D to E is probably caused by a codimension 3 bifurcation. We did not succeed to unfold this bifurcation theoretically. However out of the numerical facts a suggestion what might happen is made.
   Suppose the bifurcation occurs at point $(\tilde{F}_0, \tilde{G}_0, \tilde{\varepsilon})$ in the (F_0, G_0, ε)-space. Numerical fact is that "before" the bifurcation, that is for $\varepsilon < \tilde{\varepsilon}$, the cusp curve $C_{\varepsilon<\tilde{\varepsilon}} = SN_1 \cap SN_2$. While "after" the bifurcation, that is for $\varepsilon > \tilde{\varepsilon}$, $C_{\varepsilon>\tilde{\varepsilon}} = SN_1 \cap SN_3$. See figure 33 for the configuration of the saddle-node curves before and after the bifurcation. This numerical fact is analogous to a cusp bifurcation of two saddle-node curves in the parameter-plane. From figure 7 we recall that if two saddle-node curves collide in a cusp, then at one curve, "before" the cusp, the fixed points x_1 and x_2 collide, while at the other curve, "after" the cusp the fixed points x_1 and x_3 collide.
   So the suggestion is that two cusp bifurcation curves becomes tangent to each-other, meaning that the three saddle-node surfaces involved become tangent to each-other and we call this bifurcation a *cusp saddle-node bifurcation* (CSN). The bifurcation can not occur in one dimension, but the normal form has to be a two dimensional map. More theoretical and numerical investigations have to be done to unfold this bifurcation completely.

3. The transition from structure F to structure G is not investigated.

Within each global structure also local bifurcations of codimension 2 and 3 occur. These local bifurcations are discussed below for each structure group. Most of them are cusp or dovetail bifurcations, compare Broer, Simó and Tatjer and the figures 7 and 8. A local bifurcation is only described when it differs from the bifurcations in the structures before.

Structure A: Diagrams of the cases $\varepsilon = 0.1$ and $\varepsilon = 0.18$

1. SN_{7-8} meets 1 cusp, denoted by C_1
2. SN_{5-6} meets 3 cusp bifurcations, denoted by C_2, C_3 and C_4. C_3 and C_4 belong to a dovetail area, denoted by D_{C_3,C_4}. See for a magnification of this area in the case $\varepsilon = 0.1$, figure 32 (left).

Structure **B**: Diagrams of the cases $\varepsilon = 0.19$, $\varepsilon = 0.2$ and $\varepsilon = 0.26$

1. SN_{4-5} meets the same bifurcations as SN_{5-6} of structure A.
2. In the cases $\varepsilon = 0.2$ and $\varepsilon = 0.26$, SN_{2-6} meets 2 cusp bifurcations, denoted by C_5 and C_6. They belong to a dovetail area, denoted by D_{C_5,C_6}. See for a magnification of this area in the case $\varepsilon = 0.2$, figure 32 (middle).

Structure **C**: Diagrams of the cases $\varepsilon = 0.28$ and $\varepsilon = 0.3$

1. SN_{1-2} meets cusp C_5, that belonged to dovetail area D_{C_5,C_6} on SN_{2-6} of structure B
2. In the case $\varepsilon = 0.3$, SN_{1-2} meets two more cusp bifurcations, denoted by C_7 and C_8. They belong to a dovetail area, denoted by D_{C_7,C_8}. See for a magnification of this area and C_5 , figure 32 (right).
3. SN_{3-6} meets cusp C_6, that belonged to dovetail area D_{C_5,C_6} on SN_{2-6} of structure B

Structure **D**: Diagrams of the cases $\varepsilon = 0.305$, $\varepsilon = 0.32$ and $\varepsilon = 0.35$

1. SN_{2-8} meets cusp C_1, that belonged to SN_{7-8} of structure A, B and C.
2. In the case $\varepsilon = 0.305$, SN_{1-7} meets the same bifurcations as SN_{1-2} of structure A. But for $\varepsilon = 0.32$ and $\varepsilon = 0.35$ these bifurcations have disappeared.
3. In the case $\varepsilon = 0.35$, cusp C_4 of D_{C_3,C_4} has moved to a place where $F_0 > 20.5$. This is only a quantitative change.
4. In the case $\varepsilon = 0.35$, SN_{1-7} meets 2 cusp bifurcations, denoted by C_9 and C_{10}. They belong to a dovetail area, denoted by $D_{C_9,C_{10}}$.

Structure **E**: Diagram of the case $\varepsilon = 0.374$

1. SN_{3-8} meets cusps C_6 and C_1 that respectively belonged to SN_{3-6} and SN_{2-8} of structure D.
2. SN_{9-10} has entered the investigated (F_0, G_0)-region.

Structure **F**: Diagrams of the cases $\varepsilon = 0.3745$, $\varepsilon = 0.4$ and $\varepsilon = 0.45$

1. In the case $\varepsilon = 0.3745$, SN_{7-10} meets dovetail area $D_{C_9,C_{10}}$ that belonged to SN_{1-7} of structure D ($\varepsilon = 0.35$), E.
2. In the cases $\varepsilon = 0.4$ and $\varepsilon = 0.45$, SN_{7-10} does not cross itself anymore. Consequence is that the dovetail $D_{C_9,C_{10}}$ has disappeared. Only the two (separated) cusps, C_9 and C_{10} remain.
3. In the cases $\varepsilon = 0.45$, SN_{2-6} meets 3 cusp bifurcations, denoted by C_{11}, C_{12} and C_{13}. These cusps bound a relatively large area in the (F_0, G_0) plane. Whether some of these cusps belong to some area, for example a dovetail area, is not investigated yet. If ε is decreased a little, for example $\varepsilon = 0.448$, SN_{2-6} meets no bifurcations, like in the case $\varepsilon = 0.4$.

Structure **G**: Diagram of the case $\varepsilon = 0.5$

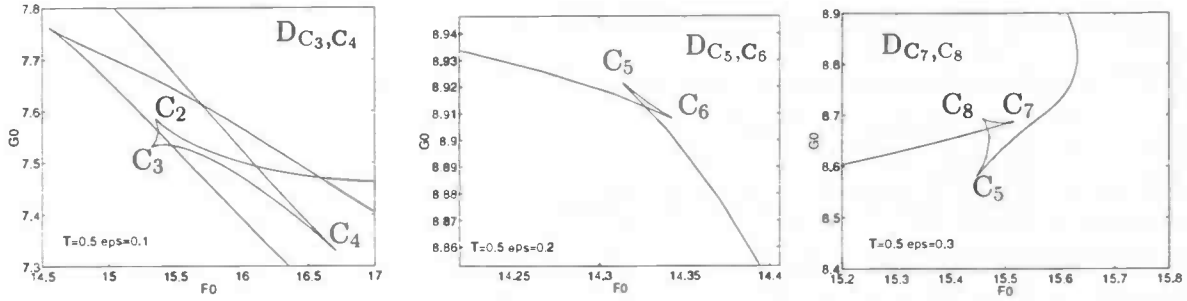

Figure 32: Driven Lorenz-84 system with $T = 0.5$ and respectively $\varepsilon = 0.1$, $\varepsilon = 0.2$ and $\varepsilon = 0.3$: magnification of dovetail areas in the (F_0, G_0)-plane at the boundaries of the Arnol'd tongues with $\rho = \frac{3}{5}$.

Figure 33: Driven Lorenz-84 system with $T = 0.5$ and $\varepsilon = 0.37$ respectively $\varepsilon = 0.374$: The $SN^{(5)}$ curves and the cusp $C^{(5)}$ before and after the codimension 3 bifurcation.

1. The cusp C_{12} on SN_{2-6} of structure F has moved to a position with $F_0 > 20.5$, thereby forming two "new" ends, 11 and 12. In the case $\varepsilon = 0.48$ this cusp still exists. But in the case $\varepsilon = 0.5$ the cusp does not exist anymore. Furthermore SN_{6-11} and SN_{2-12} are disconnected now. In which sort of bifurcation this happens has not been investigated yet.

Remarks

1. The structure of the Arnol'd tongue with $\rho = \frac{3}{5}$ changes also outside the (F_0, G_0) region of seize $(8, 20.5) \times (6, 12)$. Again this has not been investigated yet.

2. The structure of the Arnol'd tongue with $\rho = \frac{3}{5}$ in the neighbourhood of the related Hopf curve H is in accordance with the theory, see subsection 2.4. The tongue is wider at further distance of H that is as F_0 is larger. Furthermore the tongue is flat for $\varepsilon \to 0$.

3. The codimension 2 and 3 bifurcations on the SN curves occur generically "inside" a tongue. This is logical because at least three different period 5 orbits are involved in such a bifurcation. The bifurcation diagram in the case of $\varepsilon = 0.32$ shows this feature the best, see figure 30.

4. What the stability is of each period 5 orbit inside the tongue and which period 5 orbits collide at each SN curve has not been investigated yet.

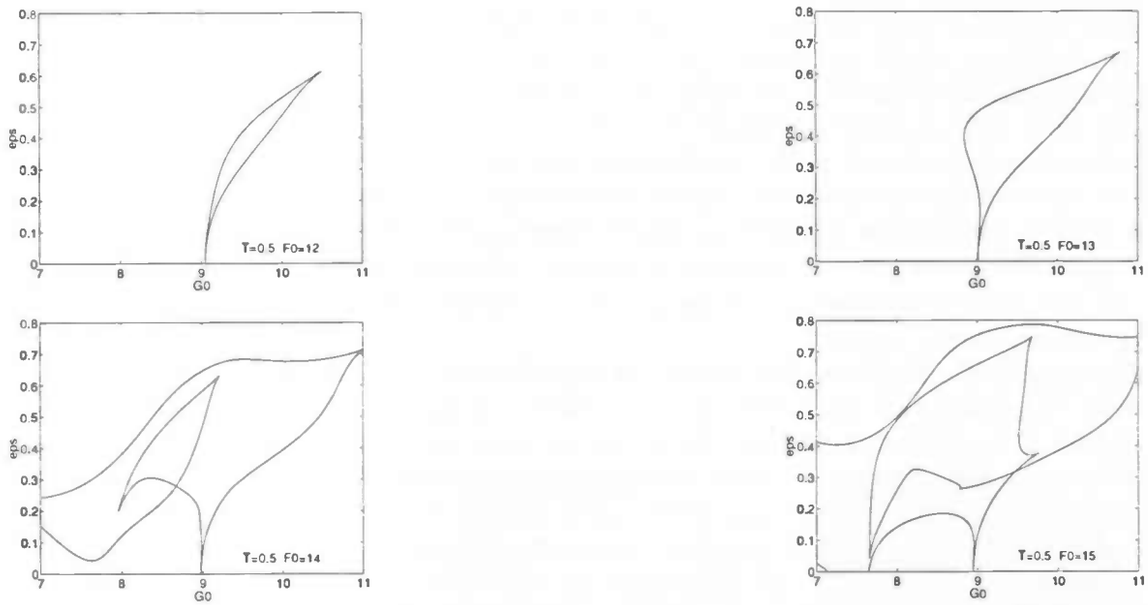

Figure 34: Driven Lorenz-84 with $T = 0.5$ and respectively $F_0 = 12$, 13, 14 and 15 : the boundaries of the Arnol'd tongues with $\rho = \frac{3}{5}$ in the (G_0, ε)-plane.

5. One can easily derive the number of period 5 orbits inside each region of the Arnol'd tongue with $\rho = \frac{3}{5}$ by just looking at which side of a saddle-node curve two more period 5 orbits show up. Outside the tongue zero period 5 orbits exist and in the tongue regions are where two, four, six and even eight different period 5 orbits exist, see figure 30.

Also the tongue boundaries have been determined in the (G_0, ε)-plane for fixed values of F_0, see figure 34. We see that if $\varepsilon \to 0$ the width of the tongue becomes independent of the value of F_0, i.e. independent of the distance to the H curve. The theoretical expectation that the Arnol'd tongue is flat in ε is confirmed. In the neighbourhood of the H curve, when $F_0 = 12$ or $F_0 = 13$ the tongue boundaries are as expected. The boundaries meet each other at $\varepsilon = 0$ on the tongue "hair", probably both boundaries have infinite order of contact. For $\varepsilon > 0$ the boundaries meet on the H curve. The tongue boundaries become more complicated at larger distance of the H curve. At $F_0 = 14$ and $F_0 = 15$ the boundaries also meet for $\varepsilon = 0$ probably again with infinite order of contact and for $\varepsilon > 0$ on the H curve. But when $F_0 = 14$ one tongue boundary has a complicated structure between these two points. It meets two cusp bifurcations and exists also for G_0 smaller than 7. For $F_0 = 15$ one boundary meets four cusps and the other boundary even transverses the line $\varepsilon = 0$. Conclusion is that the tongue boundaries are like expected at small distance from the H_ε curve with ε small. However, when the distance (or ε) is increased they become more complicated, probably because there are more than two periodic orbits on the invariant circle, compare also figure 30.

7.3 Destruction of the invariant circle

In this subsection we present two routes to chaos, found in the driven Lorenz-84 system with $T = 0.5$. Both routes begin with periodic behaviour on an invariant circle and end with

chaotic behaviour around a destroyed invariant circle.
First we discuss some bifurcations of period 5 orbits inside the Arnol'd tongue with $\rho = \frac{3}{5}$. At $(F_0, G_0) = (12, 10)$ two period 5 orbits exist on the invariant circle, see figure 35(a). When F_0 is increased, fixing $G_0 = 10$, the period 5 orbits themselves undergo bifurcations.
For $F_0 = 12.85$ a period doubling bifurcation of the period 5 saddle orbit is detected. This bifurcation is continued in the (F_0, G_0)-plane, see curve $\mathrm{PD}^{(5)}$ in figure 36. It is striking that the curve is closed and is almost tangent at both tongue boundaries. At the points of tangency a possible codimension 2 bifurcation occurs where a period 5 orbit simultaneously undergoes a saddle-node and a period doubling bifurcation. The corresponding fixed point of the map $f^{(5)}_{\varepsilon,\alpha}$ has then eigenvalues $\mu_1 = 1$ and $\mu_2 = -1$. Further research at these (codimension 2) points is needed.
The period 10 orbit that exists inside the region enclosed by the $\mathrm{PD}^{(5)}$ curve is of saddle-type. Therefore it is not possible to detect this orbit just studying the Poincaré map with `DsTool` [14]. Behind the region, the period 10 orbit undergoes a inverted period-doubling bifurcation and the period 5 orbit of saddle-type reappears. This orbit undergoes another period doubling bifurcation, around $F_0 = 18.5$, thereby creating a period 10 orbit of saddle-type. This bifurcation is continued also in the (F_0, G_0)-plane, see curve $\mathrm{PD}^{(5)}_2$ in figure 36.
Also the unstable period 5 orbit, existing at $(F_0, G_0) = (12, 10)$, undergoes a bifurcation when F_0 is increased. The unstable period 5 orbit undergoes a Hopf bifurcation for $F_0 = 13.59$ where it becomes of saddle-type and a unstable quasi-periodic repellor consisting of 5 invariant circles appears, see figure 35(b) for such a repellor. Also this bifurcation is continued in the (F_0, G_0)-plane, see curve $\mathrm{H}^{(5)}$ in figure 36.
$\mathrm{H}^{(5)}$ ends at both sides at a $\mathrm{SN}^{(5)}$ curve. Probably the period 5 orbit undergoes a Bogdanov-Takens bifurcation at both places, see sub-subsection 2.2.1. Further research at these points is still needed.
Again Arnol'd tongues are expected to emerge from this $\mathrm{H}^{(5)}$ curve. When $\mathrm{H}^{(5)}$ indeed ends in $\mathrm{BT}^{(5)}$ bifurcations at both sides, the whole range of Arnol'd tongues with rotation number varying form 0 to 1 will be present. Maybe their boundaries can be determined in future research. Inside the tongues will be frequency locking on the period 5 circles and periodic repellors will show up with period a multiple of 5. Such repellors are detected with `DsTool` [14], see figure 35(c) for a period 35 repellor. At a distance of the $\mathrm{H}^{(5)}$ curve, the 5 invariant circles are destroyed and a chaotic repellor appears, see figure 35(d-e-f) for some chaotic repellors. A magnification of one of the five regions of the chaotic repellor, such as in figure 35(4), makes clear that it has a Hénon-like structure, see figure 37. So the chaotic repellor is created by folding of the unstable manifolds of a period 5 orbit of saddle type.

Remarks

1. The points in the (F_0, G_0)-plane where the bifurcation curves $\mathrm{PD}^{(5)}$ and $\mathrm{H}^{(5)}$ cross each other are no codimension 2 points in the product of the parameter- and phase-space. Because the curves belong to two different periodic orbits, namely the period 5 saddle orbit and the unstable period 5 orbit.

2. The curves $\mathrm{SN}^{(5)}$ and $\mathrm{PD}^{(5)}$ laying close together this is also seen in the tongues of the fattened Arnol'd map, see Broer, Simó and Tatjer [7].

Finally we show some practical results obtained in the neighbourhood of the region where the Arnol'd tongues with rotation numbers $\rho = \frac{3}{5}$ and $\rho = \frac{4}{7}$ overlap. These tongues overlap when $\varepsilon = 0.5$, see figure 29(right). $F_0 = 13$ is taken fixed and for several values of G_0 we

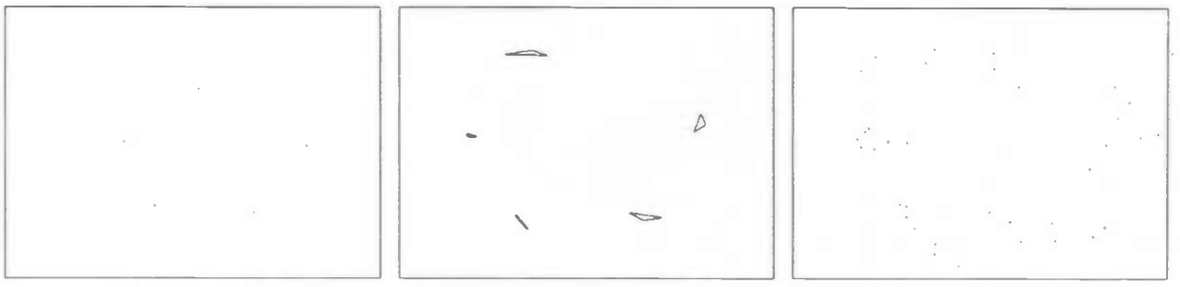

(a) $(F_0, G_0) = (12, 10)$ (b) $(F_0, G_0) = (13.625, 10)$ (c) $(F_0, G_0) = (13.62, 9.8)$

(d) $(F_0, G_0) = (13.67, 10)$ (e) $(F_0, G_0) = (13.9, 10)$ (f) $(F_0, G_0) = (14.3, 10)$

Figure 35: Driven Lorenz-84 system with $T = 0.5$ and $\varepsilon = 0.5$: a projection of repellors at (F_0, G_0)-values inside the Arnol'd tongue with $\rho = \frac{3}{5}$ onto the (Y, Z)-plane of seize $(-1.6, 1) \times (0.6, 3.1)$

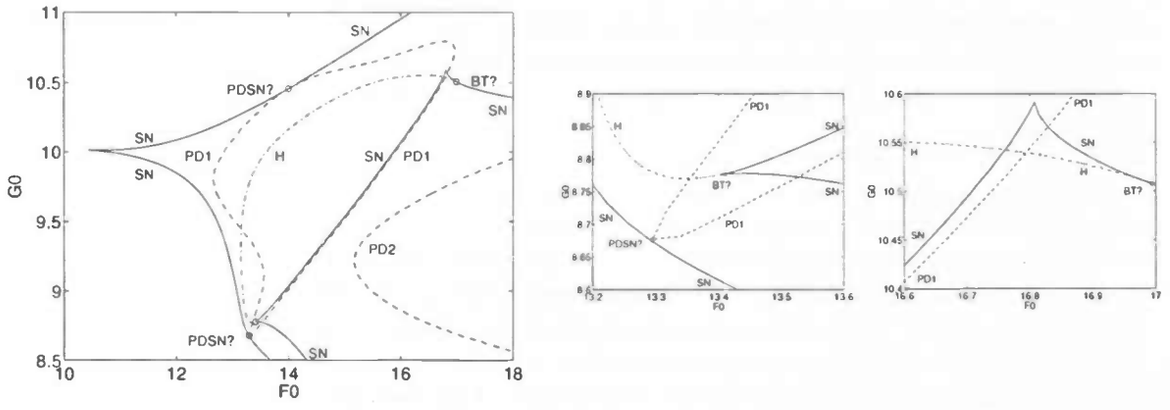

Figure 36: Driven Lorenz-84 system with $T = 0.5$ and $\varepsilon = 0.5$: bifurcation curves of period 5 orbits inside the Arnol'd tongue with $\rho = \frac{3}{5}$; And magnifications of the both regions where a Bogdanov-Takens bifurcation (BT?) is expected. The $SN^{(5)}$ curves (SN) are solid, the $PD^{(5)}$ curves (PD1 and PD2) are dashed and the curve $H^{(5)}$ (H) is dash-dotted, the two probably codimension 2 points where a $PD^{(5)}$ curve is tangent to a $SN^{(5)}$ curve are indicated (PDSN?).

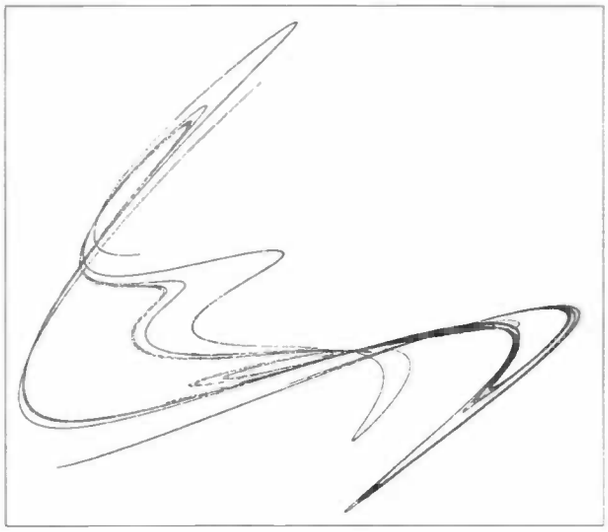

Figure 37: Driven Lorenz-84 system with $T = 0.5$, $\varepsilon = 0.5$ and $(F_0, G_0) = (16.815, 10.5)$: a magnification of one of the five regions of the chaotic repellor, such as in figure 35(4). Projection on the (Y, Z)-plane of seize $(-1.78, -1.42) \times (2.7, 2.94)$. The repellor clearly has a Hénon-like structure.

look at the repellors of the map $f_{\varepsilon,\alpha}$. For $G_0 = 9.147$ a period 5 orbit exists on S. But at $G_0 = 9.146$ a large Viana-like repellor appears and S is destroyed, see Broer, Simó and Tatjer [7] and its references. For $G_0 = 8.944$ this chaotic repellor still exist. But for $G_0 = 8.943$ S reappears and a period 7 repellor on S is found. See figure 38 for projection of these repellors on the (Y, Z)-plane.

Remark

To get more insight in the structure of the chaotic repellors it sometimes can be useful to make a "Poincaré map" of the Poincaré map by taking as cross section a small slight times a half plane. for example take as section in the (X, Y, Z)-space: $\Sigma := \{[x, x + \varepsilon^*] \times \mathbb{R}^+ \times \mathbb{R}\}$, with $\varepsilon^* \ll 1$.

7.4 Conclusion

Periodic forcing with period $T = 0.5$ has great influence on the Lorenz-84 system. For this period Arnol'd tongues are found with their typical behaviour. With `DsTool` [14] all sort of repellors are found: fixed points, quasi-periodic and periodic orbits on invariant circles, and chaotic orbits round destroyed invariant circles. The routes to chaos occur inside the Arnol'd tongues, as well as at their boundaries. The results of our investigation with `AUTO` [11] of the Arnol'd tongue with $\rho = \frac{3}{5}$ explains the tongue structure in a large part of the parameter space (F_0, G_0, ε).

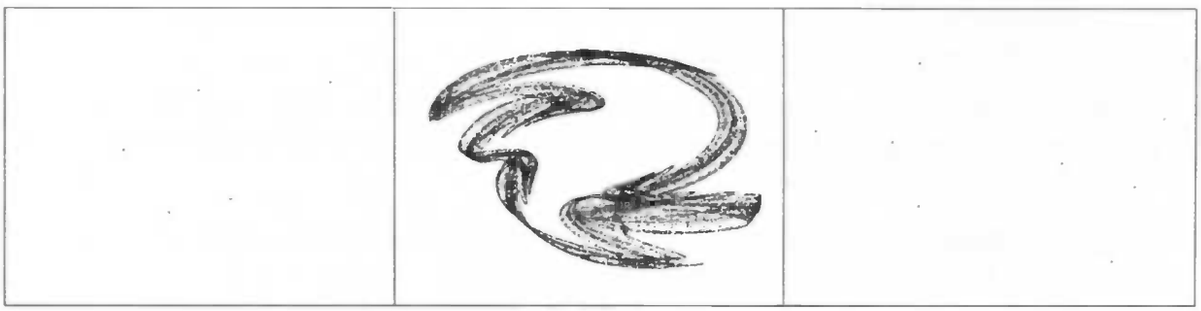

Figure 38: Driven Lorenz-84 with $T = 0.5$, $\epsilon = 0.5$ and $F_0 = 13$, varying G_0 from the Arnol'd tongue with $\rho = \frac{3}{5}$ to the one with $\rho = \frac{4}{7}$: Viana-like chaotic repellors appear in the neighbourhood of the tongue boundaries.

8 Conclusions

The driven Lorenz-84 system exhibits complicated behaviour. A first exploration of the system with the packages AUTO [11] and DsTool [14] clearly shows this. However cases with different periods of forcing are investigated with different success.

1. The period $T = 0.5$ greatly influences and changes the Lorenz-84 system. For this period Arnol'd tongues are found with their typical behaviour, see Broer, Simó and Tatjer [7]. They structure a large part of the parameter space (F_0, G_0, ϵ). The boundaries of the largest tongue ($\rho = \frac{3}{5}$) are continuated with AUTO [11]. The results show the complicated global structure of the tongue. With DsTool [14] all kinds of repellors in and around tongues are found: fixed points, periodic orbits on invariant circles, quasi-periodic orbits and chaotic orbits around destroyed invariant circles.

2. To investigate the driven Lorenz-84 system with year rhythm (that is forcing period $T = 73$) specialized tools with higher accuracy are needed. However, frequency locking and tongue-structure can be found using a high order method based on direct Taylor expansion.

3. All previously mentioned complicated behaviour has to be present in the driven Lorenz-84 system with day rhythm (that is forcing period $T = 0.2$). However, perhaps due to the small scale on which such dynamics occurs, we have not yet been able to find it numerically. No influence of day rhythm on the Lorenz-84 system is detected with DsTool [14] and AUTO [11], probably because the period the period of forcing is small compared to the characteristic periods of the Lorenz-84 system.

The results of C.Simó on the system with year rhythm ($T = 73$) and our present results for period $T = 0.5$ strongly suggest further studies. They studies can be divided in different areas. We think that a mixture of theoretical and numerical studies will be most fruitful.
The following suggestions are related to the studies of maps in general:

1. Unfolding of the codimension 2 and 3 bifurcations on the Arnol'd tongue boundaries, see for example the results obtained at the fattened Hénon map by Broer, Simó and Tatjer, [7].

2. Unfolding of the codimension 3 cusp saddle-node bifurcation, which is found on the boundaries of the Arnol'd tongue with $\rho = \frac{3}{5}$ in the driven Lorenz-84 system with $T = 0.5$, see figure 30.

3. Unfolding of the codimension 2 period-doubling saddle-node bifurcation, which is found on the boundaries of the Arnol'd tongue with $\rho = \frac{3}{5}$ in the driven Lorenz-84 system with $T = 0.5$, see figure 36.

4. Computing two-dimensional unstable manifolds of saddle-points, for example using one of the methods of Krauskopf and Osinga, see [18].

5. Looking at the chaotic attractors of $f_{T,\varepsilon,\alpha}$ in the 3-dimensional space with a visualization package.

6. Looking for 3D chaotic attractors, their theory is in progress by Tatjer.

The following suggestions are specific for studies of the driven Lorenz-84 system:

1. Determining bifurcation curves, especially the Hopf curve and tongue boundaries in the (F_0, G_0)-plane of the driven Lorenz-84 system with year rhythm.

2. Determining bifurcation curves of the period 5 orbits inside the Arnol'd tongue with $\rho = \frac{3}{5}$ for different values of ε.

3. Determining Arnol'd tongues emerging from the $H^{(5)}$ curve inside the Arnol'd tongue with $\rho = \frac{3}{5}$, i.e. continuation of boundaries of the tongues corresponding to orbits with period a multiple of 5.

4. Investigating the influence of other periods T on the driven Lorenz-84 system and making limit set diagrams for $T = 0.2$ and $T = 0.2$ like is done for $T = 73$ (figure 23) and comparing these diagrams.

5. Making another "Poincaré map" on the chaotic attractors to obtain, a set in the 2-dimensional plane. This may give more insight in the structure of the attractor.

6. Performing a data-analysis and investigating power spectra, dimensions, Lyapunov exponents etcetera.

Furthermore some investigations in the meteorological area are still needed:

1. Getting a derivation of the Lorenz-84 model out of the partial Navier-Stokes equations for a better meteorological interpretation of the results, see Saltzman [31].

2. Comparing the numerical found features with meteorological data. The question is whether you see something of the interesting dynamics of the driven Lorenz-84 system in meteorological data.

References

[1] L. Anastassiades, *Numerical Studies on the Lorenz-84 Atmosphere Model*, K.N.M.I., Scientific report; WR 95-05 (1995).

[2] V. I. Arnol'd, *Small denominators*, I. Transl. Amer. Math. Soc. 2nd. series **46**, 213-284 (1965).

[3] H. W. Broer, J. van der Craats, F. Verhulst, *Het einde van de voorspelbaarheid?* Epsilon Uitgaven, Utrecht (1995).

[4] H. W. Broer, K. W. Homan, I. Hoveijn and B. Krauskopf, *Subject: The organizing centers in the parameter plane of the Lorenz-84 system*, To appear.

[5] H. W. Broer, G. B. Huitema and M. B. Sevryuk, *Quasi-periodic motions in families of dynamical systems*, Springer-Verlag LNM 1645 (1996).

[6] H. W. Broer, R. Roussarie, C. Simó, *On the Bogdanov-Takens bifurcation for planar diffeomorphisms*, Proc. Equadiff 91, 81-92, WOrld Scientific (1993).

[7] H. W. Broer, C. Simó, J.C. Tatjer, *Towards global models near homoclinic tangencies of dissipative diffeomorphisms*, Nonlinearity **11**, 667-770 (1998).

[8] H. W. Broer, C. Simó, *The periodically driven Lorenz-84 model: a study of seasonal effects*, In preparation.

[9] H. W. Broer, F. Verhulst, *Dynamische Systemen en Chaos, een revolutie vanuit de wiskunde*, Epsilon Uitgaven, Utrecht (1992).

[10] R. L. Devaney, *An Introduction to Chaotical Dynamical Systems. Second edition*, Addison-Wesley, USA (1989).

[11] E. Doedel, T. Fairgrieve, X. Wang, AUTO94: **Software for Continuation and Bifurcation Problems in Ordinary Differential** Equations, Center for Research on Parallel Computing, California Institute of Technology (1996).

[12] P. Glendinning, C. Sparrow, *Local and Global Behaviour near Homoclinic Orbits*, Journal of Stastistical Physics, Vol. 35 (1984).

[13] J. Guckenheimer, Ph. Holmes, *Nonlinear Oscillations, Dynamical Systems, and Bifurcations of Vector Fields*, Springer-Verlag, New York, USA (1983).

[14] J. Guckenheimer, M. Myers, F. Wicklin, P. Worfolk, DsTool: A Dynamical System **Toolkit with an Interactive Interface**, Center for Applied Mathematics, Cornell University (1991).

[15] K. Homan, R. Kock, *Logboek Dynamische Exploraties*, Unpublished (1996).

[16] K. W. Homan, *Routes to chaos in the Lorenz-84 atmospheric model* Master's Thesis, University of Groningen (1997).

[17] B. Krauskopf, *On the 1:4 Resonance Problem: Analysis of the Bifurcation Set*, Ph.D. Thesis, University of Groningen (1995).

[18] B. Krauskopf and H.M. Osinga, *Globalizing two-dimensional unstable manifolds of maps*, Int. Journal of Bifurcation and Chaos, Vol. 8, No. 3, 483-503 (1998).

[19] Y. Kuznetsov, *Elements of Applied Bifurcation Theory*, Springer-Verlag, New York, USA (1995).

[20] E. Lorenz, *Low-order Models of Atmospheric Circulations*, Journal of the Meteorological Society of Japan, Vol.60, No.1, 255-267 (1982).

[21] E. Lorenz, *Irregularity: a fundamental property of the atmosphere* Tellus, 36A, 98-110 (1984).

[22] E. Lorenz, *Can chaos and intransitivity lead to interannual variability?*, Tellus, 42A, 378-389 (1990).

[23] A. Sicardi Schifino, C. Masoller, *Analytical Study of the Codimension Two Bifurcations of the New Lorenz System* Instabilities and Nonequilibrium Structures V, 345-348 (1996).

[24] S. Newhouse, J. Palis, F. Takens, *Occurence of strange axiom A attractors near quasi periodic flows on T^m, $m \leq 3$*, Comm. Math. Phys. **64**, 35-40 (1978).

[25] J. Palis and F. Takens, *Hyperbolicity & sensitive chaotic dynamics at homoclinic bifurcations*, Cambridge studies in advanced mathematics 35 (1993).

[26] H.-O. Peitgen, H. Jürgens, D. Saupe, *Chaos and Fractals, New Frontiers of Science*, Springer-Verlag (1992).

[27] D. Ruelle, F. Takens, *On the nature of turbulence*, Comm. Math. Phys. **20**, 167-192 (1971).

[28] D. Ruelle, F. Takens, *Note concerning our paper "On the nature of turbulence"*, Comm. Math. Phys. **23**, 343-344 (1971).

[29] D. Ruelle, *Elements of Differentiable Dynamics and Bifurcation Theory*, Academic Press, INC. (1988).

[30] D. Ruelle, *Chaotic Evolution and Strange Attractors*, Cambridge University Press (1987).

[31] B. Saltzman, *Folded resonance and seasonal vacillation in a thermally forced baroclinic wave model*, Atmósfera **2**, 131-154 (1989).

[32] A. Shil'nikov, G. Nicolis, C. Nicolis, *Bifurcation and Predictability Analysis of a Low-order atmospheric Circulation Model*, Int. Journal of Bifurcation and Chaos, Vol. 5, No. 6, 1701-1711 (1995).

[33] G. Zondervan *Chaos and Coupling: A coupled atmosphere ocean-boxmodel for coupled behaviour studies*, K.N.M.I., Scientific report; WR 96-02 (1996).